ORIGINAL ARTICLE

Immunosuppressive Effects of Tacrolimus on Macrophages Ameliorate Experimental Colitis

Takuya Yoshino, MD, Hiroshi Nakase, MD, PhD,* Yusuke Honzawa, MD,* Kayoko Matsumura, MD,* Shuuji Yamamoto, MD,* Yasuhiro Takeda, MD,* Satoru, Ueno, MD,* Norimitsu Uza, MD,* Satohiro Masuda, MD, PhD,† Kenichi Inui, MD, PhD,† and Tsutomu Chiba, MD, PhD**

Background: Tacrolimus is a novel immunomodulator for inflammatory bowel diseases. Immunosuppressive effects of tacrolimus on T cells are well known; however, the effects of tacrolimus on macrophages remain unclear. The aim of this study was to investigate the effects of tacrolimus on activated macrophages and to examine its efficacy in murine colitis models.

Methods: Proinflammatory cytokine production from lipopolysaccharide (LPS)–stimulated peritoneal macrophages of IL-10-knockout (KO) mice with and without tacrolimus was measured. We investigated the effects of tacrolimus on nuclear factor-κB (NF-κB), mitogen-activated protein kinase (MAPK), and caspase activation in macrophages and the induction of apoptosis in macrophages in vitro and examined the in vivo apoptotic effect of tacrolimus on colonic macrophages in IL-10-KO mice. We evaluated the effect of the rectal administration of tacrolimus on colonic inflammation in IL-10-KO mice and dextran sulfate sodium (DSS)–induced colitis in CB.17/SCID mice.

Results: Proinflammatory cytokine production from tacrolimus-treated macrophages was significantly lower than that from untreated cells. Tacrolimus suppressed LPS-induced activation of both NF-κB and MAPK in macrophages and induced apoptosis of macrophages via activation of caspases 3 and 9. Rectal administration of tacrolimus evoked apoptosis of colonic macrophages in IL-10-KO mice. Moreover, the rectal administration of tacrolimus ameliorated colitis in IL-10-KO mice and DSS-induced colitis in CB.17/SCID mice. Gene expression of inflammatory cytokines in colonic mucosa was significantly lower in tacrolimus-treated mice than in untreated mice.

Conclusions: Tacrolimus suppresses the function of activated macrophages and promotes their apoptosis, which may lead to the amelioration of colonic inflammation.

(Inflamm Bowel Dis 2010;16:2022–2033)

Key Words: inflammatory bowel disease, tacrolimus, macrophage, NF-κB, MAPK, apoptosis

Inflammatory bowel disease (IBD) is the chronic disease characterized by recurrent and severe inflammation of the gastrointestinal tract.[1,2] Despite recent advances in understanding the pathophysiology of IBD, therapeutic options are still limited and the management of refractory IBD is particularly challenging.[3–5]

Recent genomewide studies have shown that dysregulation of both innate and adaptive immunity are important risk factors for the development of IBD.[6] In particular, abnormalities of the genes involved in innate immunity by recognizing and/or processing bacterial components, such as *NOD2/CARD15*, *IRGM*, and *ATG16L1*, have been revealed to play critical roles in the development of IBD.[7–9] These data suggest that the control of abnormal innate-immune responses of antigen-presenting cells to commensal bacteria is important in the treatment of IBD.

Macrophages, which recognize bacteria and incorporate bacteria or their components, play a pivotal role in innate immunity.[10] Recent studies have suggested that macrophages in the intestinal mucosa are deeply involved in maintaining intestinal homeostasis and negatively regulate excess immune responses evoked by commensal bacteria.[11] Moreover, it was also reported that abnormal responses of intestinal macrophages to commensal bacteria result in chronic intestinal inflammation.[12] In agreement with these data, recent studies have suggested that macrophage-

Received for publication March 3, 2010; Accepted March 8, 2010.

From the Department of Gastroenterology & Hepatology, Graduate School of Medicine, Kyoto University, Kyoto, Japan; and †Department of Pharmacy, Kyoto University Hospital, Kyoto, Japan.

Reprints: Hiroshi Nakase, MD, PhD, Department of Gastroenterology & Hepatology, Graduate School of Medicine, Kyoto University, 54 Kawahara-cho, Shogoin, Sakyo-ku, Kyoto, 606-8507, Japan (e-mail: hiropy_n@kuhp.kyoto-u.ac.jp)

Supported by a Grant-in-Aid for Scientific Research (C) from the Ministry of Culture and Science of Japan (grant 18590677); the Kato Memorial Trust for Nambyo Research; the Shimizu Foundation for the Promotion of Immunology Research and Japan Foundation for Applied Enzymology to Hisroshi Nakase; grants-in-aid for Scientific Research (16017240, 16017249,17013051, 17659212 and 18012029) from the Ministry of Education, Culture, Sports, Science and Technology of Japan; grant-in-aid for Scientific Research (15209024 and 18209027) from JSPS; and Health and Labour Sciences Research Grants for Research on Intractable Diseases, and Research on Advanced Medical Technology (nano005) from the Ministry of Health, Labor, and Welfare, Japan (to T.C.)

DOI 10.1002/ibd.21318

Published online 28 April 2010 in Wiley Online Library (wileyonlinelibrary.com).

targeting treatment ameliorates colonic inflammation in experimental colitis models.[13,14] Thus, the regulation of abnormal responses of macrophages appears to be a promising therapeutic approach for the treatment of IBD.

Tacrolimus is a potent immunomodulator that was isolated from *Streptomyces tsukubaensis*.[15] Tacrolimus binds the tacrolimus-binding protein, and the complex inhibits the Ca^{2+}-dependent phosphatase calcineurin, thereby preventing calcineurin-dependent interleukin (IL)–2 transcription and T-cell proliferation in a manner similar to that of cyclosporine A (CyA).[16,17] Moreover, tacrolimus has been shown to down-regulate the nuclear factor-κB (NF-κB) pathway and induce apoptosis of activated T cells by activating caspase 3.[18] Because it has such potent immunosuppressive effects on T cells, tacrolimus is now widely used for prophylaxis against not only organ rejection and autoimmune diseases but also IBD,[19,20] and it is generally accepted that the therapeutic effects of tacrolimus are a result of its inhibitory effects on T-cell functions.[15,17] However, it remains unclear whether tacrolimus also has immunoregulatory effects on macrophages.

In the present study, therefore, we examined whether tacrolimus influences the function of activated macrophages and, if so, whether this effect of tacrolimus on macrophages may have beneficial roles in the treatment of IBD.

MATERIALS AND METHODS

Animals

Female IL-10-KO mice, CB.17/SCID mice, and C57BL/6 mice (Charles River Japan, Inc., Kanagawa, Japan) 8–10 weeks old were used for the experiments. They were fed standard laboratory chow and supplied drinking water ad libitum. In our animal facility, IL-10-KO mice developed colonic inflammation at approximately 10 weeks.

Reagents

The calcineurin inhibitor tacrolimus (FR900506) was provided by Astellas Pharmaceutical Inc. (Tokyo, Japan). Lipopolysaccharide (LPS, *Escherichia coli* 0127:B8) and antibody to β-actin were purchased from Sigma-Aldrich (St. Louis, MO). Antibodies to I-κBα, p65, p38, JNK, phospho-p65, phospho-p38, phospho-JNK, caspase 3, caspase 8, and caspase 9 were purchased from Cell Signaling Technology (Danvers, MA). Antibodies to rat antimouse CD11b and rat IgG_{2b} were purchased from BD Bioscience Pharmingen (San Jose, CA).

Peritoneal Macrophages Isolation and Stimulation

Peritoneal macrophages of IL-10-KO mice were elicited by intraperitoneal injection of 2 mL of 4% thioglycolate (Eiken Chemical Co., Ltd.) in distilled water. After 4 days, elicited macrophages were collected by peritoneal lavage with phosphate buffered saline (PBS), and the cells were suspended in RPMI1640 medium (Invitrogen Corp, Carlsbad, CA) supplemented with 10% heat-inactivated fetal calf serum, 100 units/mL penicillin, and 100 μg/mL streptomycin (GIBCO, Invitrogen, Grand Island, NY). A total of 1×10^5 cells were plated in a 96-well plate and incubated for 2 hours in 5% CO_2 at 37°C. After incubation, nonadherent cells were removed by washing with PBS. Macrophages were stimulated with LPS (1 μg/mL) alone or with LPS (1 μg/mL) plus tacrolimus (0.01, 0.1 mg/mL) for 24 hours in 5% CO_2 at 37°C, and the cytokine secretion in the supernatant was measured by enzyme-linked immunosorbent assay (ELISA). For measurement of IL-12/IL-23p40, tumor necrosis factor (TNF)–α and IL-6, sandwich ELISA was performed according to the manufacturer's instructions (eBioscience, San Diego, CA).

Western Blotting

For the analysis of the effects of tacrolimus on NF-κB signaling and mitogen-activated protein kinase (MAPK) in macrophages, 1×10^6 peritoneal macrophages from IL-10-KO mice were stimulated with LPS (1 μg/mL) with or without pretreatment with tacrolimus (0.1 mg/mL) for 2 hours in 5% CO_2 at 37 °C. Then, 0, 1, 5, 10, 15, 30, and 60 minutes after stimulation, the cells were washed with PBS, and nuclear and cytoplasmic protein extractions from isolated cells were performed with an NE-PER kit (PIERCE Biotechnology, Rockford, IL) according to the manufacturer's instructions. For the analysis of the effect of tacrolimus on caspase signaling in macrophages, we used 1×10^6 RAW264.7 cells, a murine macrophage cell line, with or without tacrolimus stimulation (0.1 mg/mL) for 0 and 12 hours in 5% CO_2 at 37°C. The cells were then washed with PBS, and protein extractions from isolated cells were performed. Protein content was measured by the Bradford assay (Bio-Rad Laboratories, Hercules, CA). Proteins were separated by 10% sodium dodecyl sulfate–polyacrylamide gel electrophoresis (SDS-PAGE) and transferred to nitrocellulose membranes. The membrane was blocked with Tris-buffered saline with 0.1% Tween-20 (TBS-T) and 5% skim milk for 1 hour at room temperature. Blots were incubated overnight with the primary antibody at a dilution of 1:1000 at 4°C. After incubation, the membrane was washed 3 times for 5 minutes with TBS-T and incubated in TBS-T with 5% skim milk containing antirabbit IgG antibody conjugated with horseradish peroxidase (Amersham Pharmacia Biotech, Buckinghamshire, England) at a 1:2000 dilution for 1 hour at room temperature. Immunoreactive bands were visualized using the Immobilon Western chemiluminescent HRP substrate (Millipore, Billerica, MA).

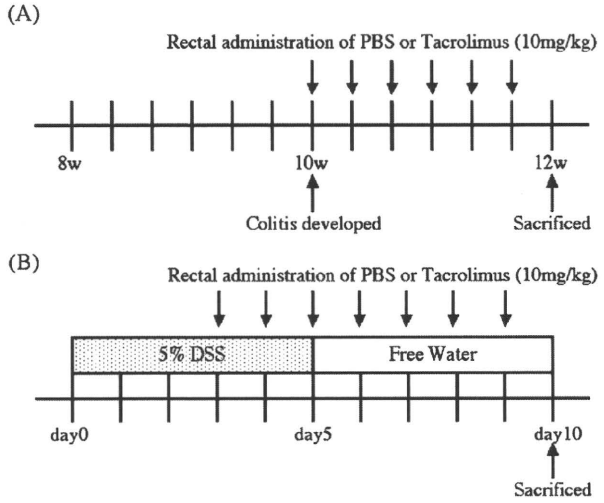

FIGURE 1. Experimental protocols of in vivo study. A: Therapeutic study using IL-10-KO mice. B: Therapeutic study using CB.17/SCID mice with DSS-induced colitis.

Evaluation of Apoptosis

To evaluate the apoptotic effect of tacrolimus on macrophages in vitro and in vivo, an Annexin V assay and a terminal deoxyribonucleotodyl tranferase-mediated dUTP-biotin nick end-labeling (TUNEL) assay were performed with an Annexin V-FITC Apoptosis Detection Kit (Bio Vision, Mountain View, CA) and an In Situ Cell Death Detection Kit (Roche Diagnostics GmbH, Mannheim, Germany), according to the manufacturers' instructions.

To evaluate the apoptotic effect of tacrolimus on macrophages, 5×10^5 RAW264.7 cells were collected 0, 1, 6, 12, and 24 hours after stimulation with tacrolimus, resuspended in 500 μL of binding buffer, and stained with Annexin V-FITC and propidium iodide at room temperature for 5 minutes in the dark. The percentage of apoptotic cells was analyzed by flow cytometry (BD Biosciences, Franklin Lakes, NJ).

Apoptosis in colonic tissue of mice treated with rectal administration of tacrolimus or PBS was detected by the TUNEL assay. IL-10-KO mice who were 12 weeks old were treated with rectal administration of tacrolimus (10 mg/kg) or PBS. Then 0, 12, and 24 hours after rectal administration of tacrolimus or PBS, mice were sacrificed, the distal colons were collected, and TUNEL staining and immunohistochemistry for CD11b were performed.

Experimental Designs of In Vivo Studies

The therapeutic studies with tacrolimus included 2 protocols, as described in Figure 1. In the first protocol, the therapeutic effect of rectal administration of tacrolimus was studied using an immune-mediated colitis model. IL-10-KO mice who were 10 weeks old were treated with rectal administration of tacrolimus (10 mg/kg) or PBS every other day 3 times a week for 2 weeks. Mice were sacrificed on day 12. As a control, 12-week-old C57BL/6 mice were also sacrificed on day 12.

In the second protocol, the therapeutic effect of the rectal administration of tacrolimus was studied in CB.17/SCID mice with dextran sulfate sodium (DSS)–induced colitis. To induce colitis in CB.17/SCID mice, 5% DSS (molecular weight 36,000–50,000 MP Biomedicals, Inc., Aurora, OH) was dissolved in water and given to CB.17/SCID mice.[21] DSS water was provided ad libitum up to 5 days. On day 5, they were switched to normal drinking water. Treatment with rectal administration of PBS or tacrolimus was performed from day 3 to day 9. Mice were sacrificed on day 10.

Evaluation of Colitis

After sacrifice, the colons of IL-10-KO and C57BL/6 mice were divided into 4 segments to represent the rectum, cecum, proximal colon, and middle colon. The histology of each segment of the colon was evaluated with hematoxylin and eosin staining. The severity of inflammation of each section was scored using a histological index ranging from 0 to 4, as previously described.[22] This index was based on the degree of epithelial layer erosion, goblet cell depletion, and inflammatory cell infiltrate [0, normal; 1, small number of inflammatory cells; 2, more extensive by number and involvement; 3, significant evidence of inflammatory infiltrate with goblet cell depletion; 4, significant evidence of inflammatory infiltrate (ulcers and crypt abscess)].

We evaluated the severity of DSS-induced colitis in CB.17/SCID mice using disease activity index (DAI) scores as described in Table 1.[23] After sacrifice, colon length was also evaluated, and the severity of inflammation of colon was scored using a histological index, as described previously.[24] Three independent parameters were measured: severity of inflammation (0–3: none, slight, moderate, and severe, respectively), depth of injury (0–3: none, mucosal, mucosal and submucosal, and transmural, respectively), and crypt damage (0–4: none, basal one-third damaged, basal two-thirds damaged, only surface epithelium intact, and entire crypt and epithelium lost, respectively). The score of each parameter was multiplied by a factor reflecting the percentage of tissue involvement (×1, 0%–25%; ×2, 26%–50%; ×3, 51%–75%; ×4, 76%–100%), and all numbers were added. The maximum possible score was 40.

Semiquantitative Analysis of Gene Expression of Proinflammatory Cytokines

Samples of colonic tissues for mRNA isolation were removed from the distal third of the colon. Total RNA was extracted using TRIzol RNA isolation reagent (Invitrogen

TABLE 1. Disease Activity Index Score

Score	Weight loss (%)	Stool consistency	Occult/gross bleeding
0	None	Normal	Normal
1	1–5		
2	6–10	Loose stool	Occult bleeding
3	11–20		
4	> 20	Diarrhea	Gross bleeding

The disease activity index (DAI) is a mean of individual scores of weight loss, stool consistency and bleeding. Normal stool = formed pellets, loose stool = pasty and semiformed stool, diarrhea = liquid stool.

Corp, Carlsbad, CA) according to the manufacturer's instructions. RNA (1 μg) was reverse-transcribed with Superscript II (Invitrogen), and the resulting complementary DNA was analyzed for IL-12/IL-23p40, TNF-α, IFN-γ, IL-17A, IL-6, and β-actin mRNA expression by semiquantitative polymerase chain reaction (PCR) using a Dyad Thermal Cycler (MJ Research, Waltham, MA). The primer sets used are described in Table 2. A 5-μL aliquot PCR product was electrophoresed on 2% agarose gel containing ethidium bromide, and the bands were examined using an image autoanalyzing system (AE-6911CX, ATTO Corp, Tokyo, Japan). The densities of bands on the gels were measured by image analysis software (CS analyzer, ATTO Corp.). Semiquantitative level of each product was corrected for the β-actin density of each sample.

Statistical Analysis

The Student t test and the Mann-Whitney U test were used where appropriate for statistical analysis. Data are expressed as means ± SDs. A P value < 0.05 was considered statistically significant.

RESULTS

Tacrolimus Inhibits Proinflammatory Cytokine Production in LPS-Stimulated Peritoneal Macrophages from IL-10-KO Mice

Macrophages are deeply involved in the onset and development of IBD.[25] Therefore, we focused on the effect of tacrolimus on macrophage function. To examine whether tacrolimus suppresses activated macrophages, we evaluated the effect of tacrolimus on proinflammatory cytokine production in LPS-stimulated peritoneal macrophages from IL-10-KO mice. As shown in Figure 2, the increases in IL-12/IL-23p40, TNF-α, and IL-6 production from peritoneal macrophages of IL-10-KO mice were all significantly inhibited by tacrolimus in a dose-dependent manner ($P < 0.001$). Thus, tacrolimus strongly suppresses LPS-stimulated inflammatory cytokine production from activated macrophages.

Tacrolimus Inhibits NF-κB and MAPK Activation Pathways

To elucidate the mechanism of the inhibitory effect of tacrolimus on proinflammatory cytokine production in LPS-stimulated macrophages, we investigated the effect of tacrolimus on the intracellular signaling pathway of peritoneal macrophages. Tacrolimus inhibited the LPS-induced degradation of I-κBα and the phosphorylation of NF-κB p65 in peritoneal macrophages from IL-10-KO mice (Fig. 3A). Furthermore, tacrolimus also inhibited LPS-induced phosphorylation of p38 and JNK in peritoneal macrophages from IL-10-KO mice (Fig. 3B). These results demonstrated that tacrolimus inhibits both the NF-κB and MAPK activation pathways induced by LPS in peritoneal macrophages from IL-10-KO mice.

TABLE 2. Primer Sets for Semiquantitative PCR

IL-12/IL-23p40	forward:	CGGTCATCTGCCGCAAA
	reverse:	TGCCCATTCGCTCCAAGA
TNF-α	forward:	TTCTGTCTACTGAACTTCGGGGTGATCGGTCC
	reverse:	GTATGAGATAGCAAATCGGCTGACGGTGTGGG
IFN-γ	forward:	TGCATCTTGGCTTTGCAGCTCTTCCTCATGGC
	reverse:	TGGACCTGTCGGGTTGTTGACCTCAAACTTGGC
IL-17A	forward:	TCTCTGATGCTGTTGCTGCT
	reverse:	CGTGGAACGGTTGAGGTAGT
IL-6	forward:	ATGAAGTTCCTCTCTGCAAGAGACT
	reverse:	CACTAGGTTTGCCGAGTAGATCTC
β-Actin	forward:	GTGGGCCGCCCTAGGCACCAG
	reverse:	CTCTTTGATGTCACGCACGATTTC

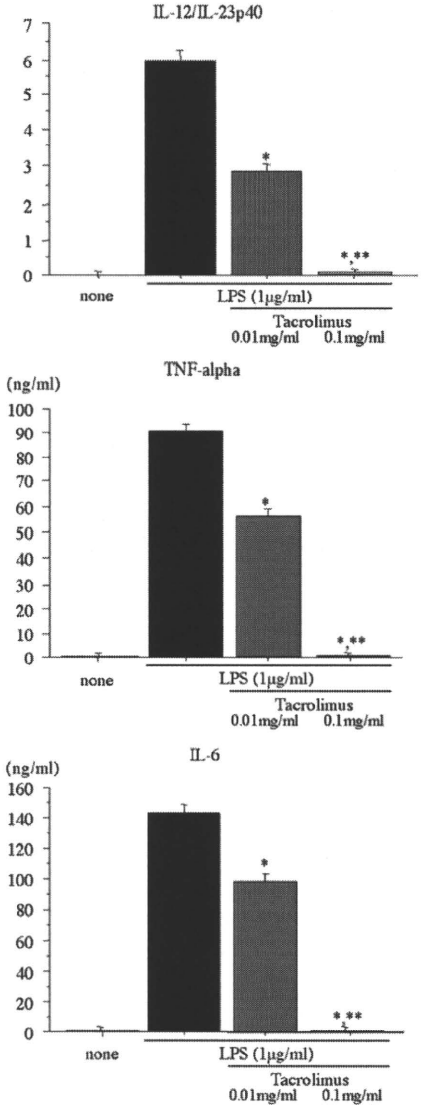

FIGURE 2. Dose-dependent effect of tacrolimus on proinflammatory cytokine production of LPS-stimulated peritoneal macrophages from IL-10-KO mice. Peritoneal macrophages from IL-10-KO mice were stimulated with medium alone or LPS (1 μg/mL) with or without tacrolimus (0.01, 0.1 mg/mL) for 24 hours, and proinflammatory cytokine secretion in the supernatant was measured by ELISA. Data are expressed as the mean ± SD ($n = 5$ in each group), and similar results were obtained in 3 independent experiments; $^{*}P < 0.001$ compared with untreated cells (LPS alone), $^{**}P < 0.001$ between tacrolimus (0.01 mg/mL) group and tacrolimus (0.1 mg/mL) group.

Tacrolimus Induces Apoptosis of Macrophages Both In Vitro and In Vivo

Induction of apoptosis in immune cells is considered one of the therapeutic strategies for IBD.[6] Therefore, we evaluated the apoptotic effects of tacrolimus on macrophages both in vitro and in vivo. As shown in Figure 4A, the percentage of annexin V–positive cells was significantly higher in RAW264.7 cells treated with tacrolimus than in those treated with PBS alone. This effect of tacrolimus was both dose- and time dependent. We also evaluated the effect of tacrolimus on caspase signaling. Tacrolimus induced activation of caspase 3 and 9, whereas it did not activate caspase 8 (Fig. 4B). These data suggested that tacrolimus-induced apoptosis of macrophages is a result of activation of the mitochondrial apoptotic pathway.

Moreover, we evaluated the in vivo apoptotic effect of rectal administration of tacrolimus on colonic macrophages in IL-10-KO mice. As shown in Figure 4C, apoptosis of colonic CD11b-positive cells in IL-10-KO mice was observed 12 and 24 hours after rectal administration of tacrolimus, whereas it was not observed in PBS-treated IL-10-KO mice. We also evaluated the in vivo apoptotic effect of tacrolimus on colonic T cells. In agreement with previous reports, tacrolimus induced apoptosis of CD4-positive T cells after 12 and 24 hours (data not shown). These in vivo data revealed that tacrolimus induces apoptosis of not only T cells but also macrophages in inflammatory colonic mucosa.

Tacrolimus Ameliorates Immune-Mediated Colitis of IL-10-KO Mice

To evaluate the therapeutic effect of tacrolimus on immune-mediated colitis, we performed the therapeutic study in IL-10-KO mice with colitis at 10 weeks. In PBS-treated IL-10-KO mice, body weight gradually decreased and did not recover during the experiment. In contrast, the body weight of tacrolimus-treated IL-10-KO mice was significantly recovered compared with that of PBS-treated IL-10-KO mice ($P < 0.05$; Fig. 5A), although there was no difference in colon length between mice with and without tacrolimus treatment (Fig. 5B). Histological findings revealed that the severe hyperplasia of colonic epithelial cells, infiltration of mononuclear cells in the colonic lamina propria, and loss of Goblet cells observed in IL-10-KO mice were significantly reduced by rectal administration of tacrolimus (Fig. 5C). Histological scores of tacrolimus-treated IL-10-KO mice were significantly lower than those of PBS-treated IL-10-KO mice ($P < 0.05$; Fig. 5D). We confirmed that indigo carmine reached the cecum after rectal administration of PBS with indigo carmine (data not shown), indicating that rectal administration of tacrolimus could be delivered throughout the colon.

Additionally, immunohistochemistry revealed that CD11b-positive cells were significantly decreased in tacrolimus-treated IL-10-KO mice compared with PBS-treated IL-10-KO mice (Fig. 6A,B). These data suggested that amelioration of colonic inflammation observed in tacrolimus-treated IL-10-KO mice involves the depletion of colonic macrophages.

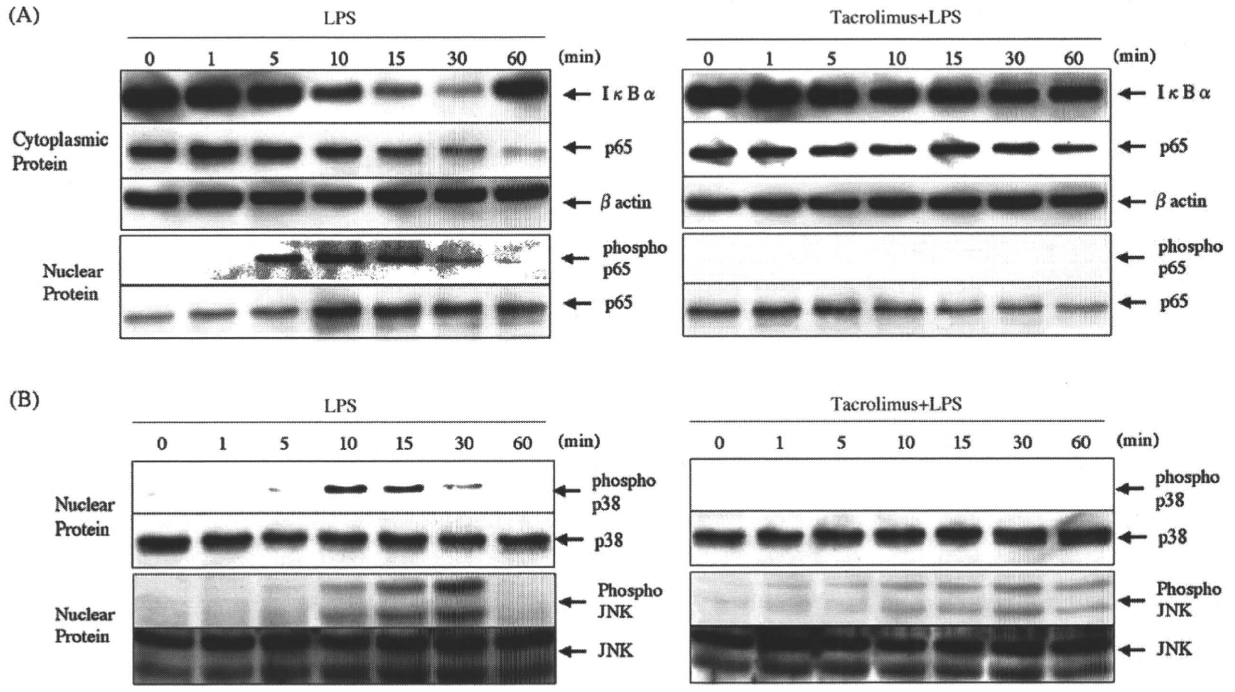

FIGURE 3. Effects of tacrolimus on NF-κB and MAPK activation in LPS-stimulated peritoneal macrophages from IL-10-KO mice. Peritoneal macrophages were stimulated by LPS (1 μg/mL) for the indicated times with (right) or without (left) pretreatment by tacrolimus (0.1 mg/mL) for 2 hours, and cell lysates were prepared and subjected to SDS-PAGE, followed by Western blot with indicated antibodies. A: Effect of tacrolimus on NF-κB activation pathway. B: Effect of tacrolimus on the MAPK activation pathway.

Tacrolimus Inhibits Gene Expression of Proinflammatory Cytokines In Vivo

To evaluate the effect of rectal administration of tacrolimus on the gene expression of proinflammatory cytokines in colonic tissues, RNA was extracted from colonic specimens of tacrolimus-treated IL-10-KO mice. As shown in Figure 7, significant increases in IL-12/IL-23p40, TNF-α, IFN-γ, IL-17A, and IL-6 transcripts were observed in the colonic tissue of IL-10-KO mice compared with those in the control mice. However, these transcripts were significantly lower in the colonic tissues of tacrolimus-treated IL-10-KO mice than in those of PBS-treated IL-10-KO mice ($P < 0.05$). These results suggested that rectal administration of tacrolimus reduces colonic inflammation of IL-10-KO mice at least in part by decreasing proinflammatory cytokines, which may be related to the depletion of colonic macrophages.

Tacrolimus Also Ameliorates DSS-Induced Colitis in CB.17/SCID Mice

To confirm whether tacrolimus-induced inhibition of macrophage functions and apoptosis contribute to the amelioration of colitis, we investigated the effect of rectal administration of tacrolimus on DSS-induced colitis in CB.17/SCID mice, which lack lymphocytes. Tacrolimus treatment significantly reduced body weight loss in CB.17/SCID mice with DSS-induced colitis (Fig. 8A). The DAI score of tacrolimus-treated CB.17/SCID mice with DSS-induced colitis was significantly lower than that of PBS-treated CB.17/SCID mice on day 10 (Fig. 8B). Macroscopically, colon length was significantly longer in tacrolimus-treated mice than in PBS-treated mice (Fig. 8C). Pathologically, tacrolimus-treated CB.17/SCID mice with DSS-induced colitis showed little cellular infiltration and regeneration of epithelial cells characterized by the presence of surface epithelium and crypt formation. In contrast, PBS-treated CB.17/SCID mice with DSS colitis showed severe cellular infiltration, loss of goblet cells, crypt damage, and mucosal ulceration (Fig. 8D). Histological scores of tacrolimus-treated CB.17/SCID mice with DSS-induced colitis were significantly lower than those of PBS-treated CB.17/SCID mice (Fig. 8E). These data suggested that apoptosis and suppression of cytokine production from macrophages induced by rectal administration of tacrolimus contribute to the amelioration of DSS-induced colitis in CB.17/SCID mice.

DISCUSSION

In this study, we examined whether tacrolimus has inhibitory effects on macrophages in addition to T cells

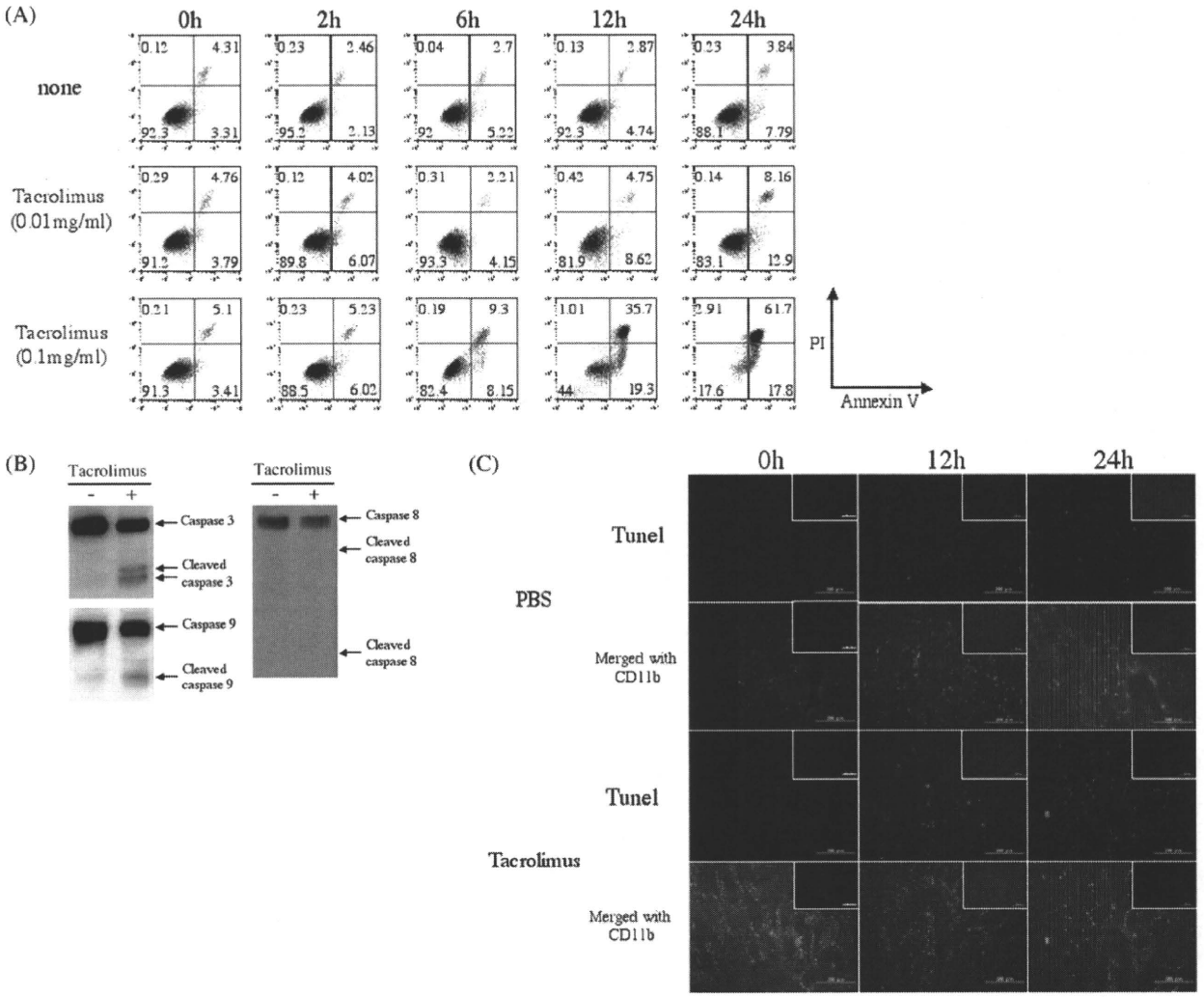

FIGURE 4. Apoptotic effects of tacrolimus on macrophages. A: Apoptotic effect of tacrolimus on a murine macrophage cell line RAW264.7. RAW264.7 cells were stimulated with or without tacrolimus (0.01 or 0.1 mg/mL) for 0, 1, 6, 12, and 24 hours. The percentage of apoptotic cells (shown at the right lower part of each panel) was analyzed by flow cytometry. Similar results were obtained in 3 independent experiments. B: Effect of tacrolimus on caspase signals. RAW264.7 cells were stimulated with or without tacrolimus (0.1 mg/mL) for 12 hours, and cell lysates were prepared and subjected to SDS-PAGE, followed by Western blot with indicated antibodies. C: In situ TUNEL assay in colonic tissue of IL-10-KO mice treated with PBS or tacrolimus. Zero, 12, and 24 hours after treatment with rectal administration of tacrolimus or PBS, TUNEL staining (TMR red labeled), and immunohistochemistry for CD11b (green) were performed on frozen sections of distal colon. Immunohistochemistry of the negative control is shown in the right upper corner (original magnification 200×). Apoptosis cells merged with CD11b were colored yellow.

and found by in vitro study that tacrolimus directly inhibited LPS-stimulated proinflammatory cytokine production in macrophages and induced apoptosis. Furthermore, we showed in vivo that rectal administration of tacrolimus attenuated colonic inflammation in both IL-10-KO mice and CB.17/SCID mice with DSS-induced colitis, which lack lymphocytes. Thus, our study demonstrated that tacrolimus directly inhibits macrophage functions and that these inhibitory effects of tacrolimus on macrophages may contribute to the therapeutic action of tacrolimus in IBD.

To evaluate the direct effects of tacrolimus on macrophages, we first investigated the effect of tacrolimus on proinflammatory cytokine production in peritoneal macrophages of IL-10-KO mice in vitro. Our results clearly demonstrated that tacrolimus directly and dose-dependently reduced LPS-induced production of IL-12/IL-23p40, TNF-

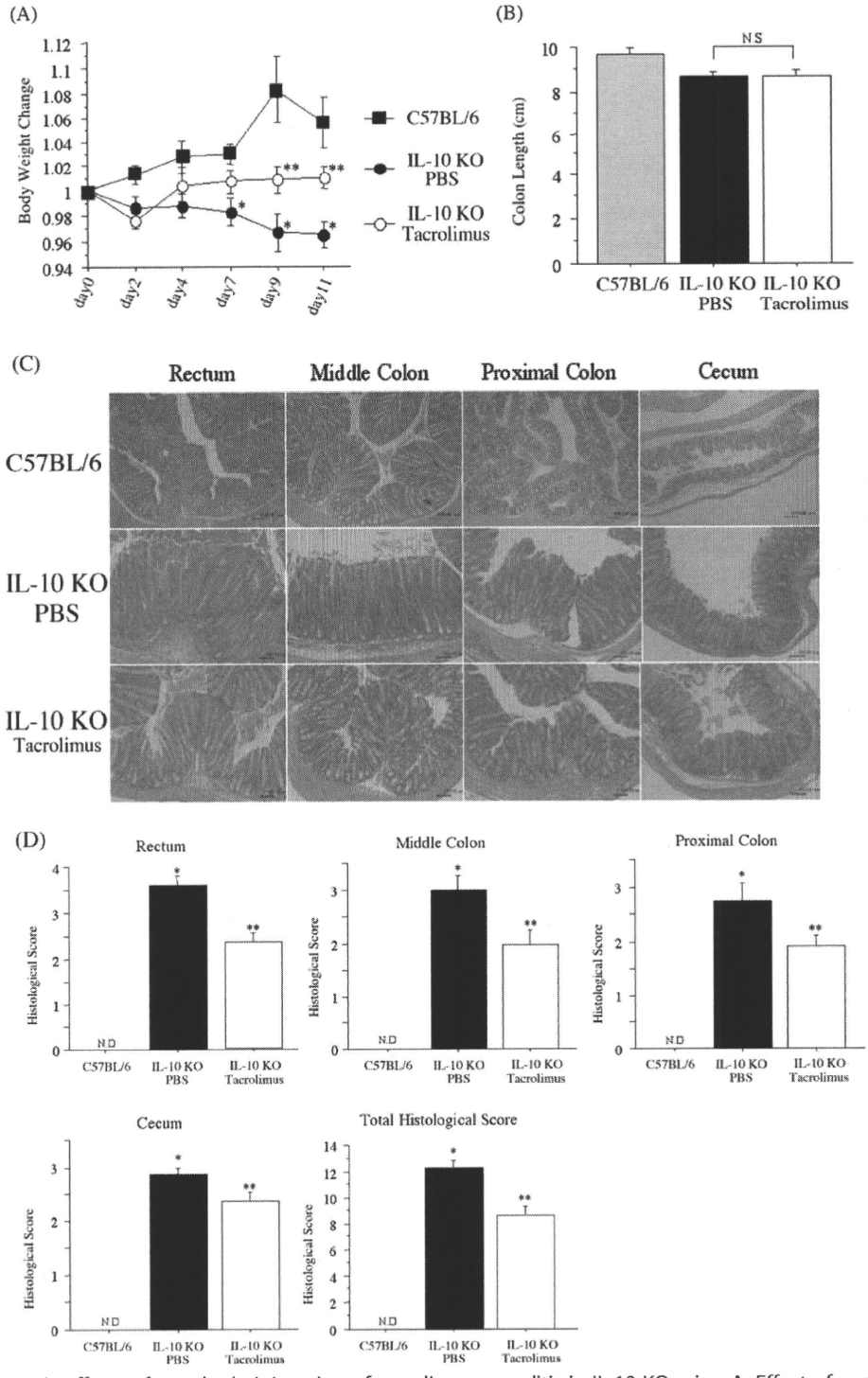

FIGURE 5. Therapeutic effects of rectal administration of tacrolimus on colitis in IL-10-KO mice. A: Effect of rectal administration of tacrolimus on body weight changes in the therapeutic study. Serial changes of body weight were measured. Data are expressed as the mean ± SD (C57BL/6 mice, $n = 3$; IL-10-KO mice, $n = 7$ in each group); $^{*}P < 0.05$ compared with C57BL/6 mice, $^{**}P < 0.05$ compared with IL-10-KO mice treated without tacrolimus (PBS alone). B: Effect of rectal administration of tacrolimus on colon length of mice. Colon length was measured from the ileocecal junction to the anal verge. Data are expressed as the mean ± SD (C57BL/6 mice, $n = 3$; IL-10-KO mice, $n = 7$ in each group). C: Representative histological findings of mice treated with rectal administration of tacrolimus or PBS (original magnification 100×). D: Histological scores of colonic tissues in mice treated with rectal administration of tacrolimus or PBS. Data are expressed as the mean ± SD (C57BL/6 mice, $n = 3$; IL-10-KO mice, $n = 7$ in each group); $^{*}P < 0.05$ compared with IL-10-KO mice treated without tacrolimus (PBS alone), $^{**}P < 0.05$ compared with C57BL/6 mice.

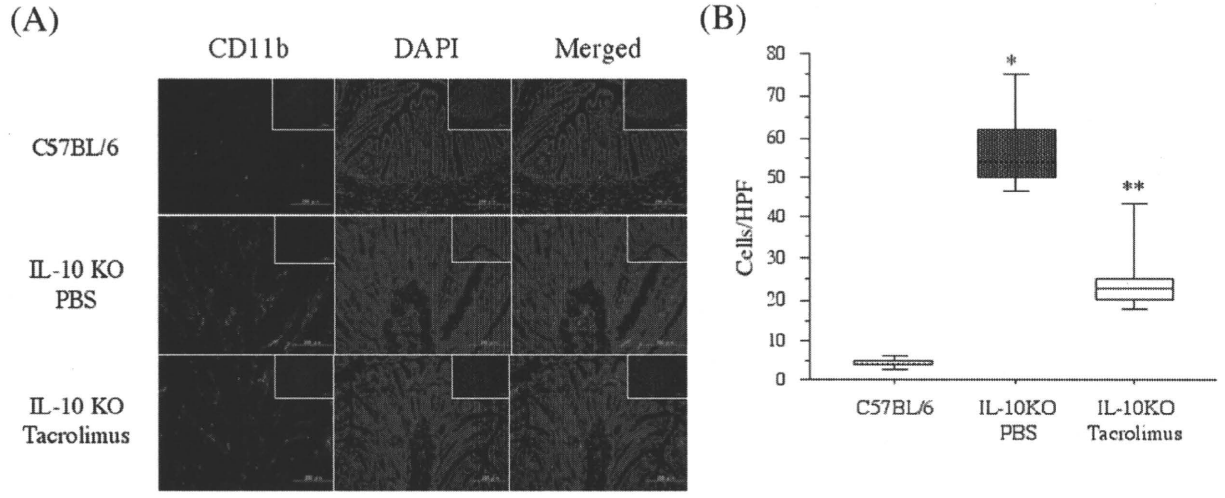

FIGURE 6. Apoptotic effects of rectal administration of tacrolimus on colonic macrophages in IL-10-KO mice. A: Immunohistochemistry for CD11b (green) and DAPI (blue) was performed on frozen sections of distal colon isolated from C57BL/6 mice and IL-10-KO mice treated with tacrolimus or PBS. Immunohistochemistry of the negative control is shown in the right upper corner (original magnification 200×). B: Cell count of CD11b-positive cells on frozen sections of distal colon isolated from C57BL/6 mice and IL-10-KO mice treated with PBS or tacrolimus. Data are expressed as the mean ± SD cell count per high-power field (HPF); $^{*}P < 0.001$ compared with C57BL/6 mice, $^{**}P < 0.05$ compared with IL-10-KO mice treated with rectal administration of PBS.

α, and IL-6 in peritoneal macrophages of IL-10-KO mice. Our data are the first to show the direct inhibitory effect of tacrolimus on the function of macrophages. Recent studies have revealed that IL-12, IL-23, TNF-α, and IL-6 play important roles in the pathophysiology of IBD.[26,27] Among them, IL-12 and IL-23 are mainly produced by activated myeloid cells such as macrophages and dendritic cells.[28] IL-12 promotes IFN-γ-producing T-cell (Th1) polarization,[29] whereas IL-23 promotes expansion of IL-17-producing T cells (Th17),[30] both of which are deeply involved in the development of IBD.[31,32] Thus, it appears reasonable that the direct inhibitory effects of tacrolimus on the production of various cytokines in macrophages as observed in this study, explain the therapeutic effect of tacrolimus on the colonic inflammation of IBD.

Tacrolimus has been reported to inhibit NF-κB activation in human $CD4^+$ T cells and keratinocytes[33] and MAPK activation in human endothelial cells.[34] Therefore, we examined the effects of tacrolimus on both NF-κB and MAPK activation in peritoneal macrophages and found that tacrolimus directly and significantly inhibited both NF-κB and MAPK activation. It is well established that activation of TLR signals by microbial components is important for macrophages to produce proinflammatory cytokines and that both the NF-κB and MAPK pathways play pivotal roles in TLR-stimulated cytokine production.[35] Indeed, Neurath et al and Zhang et al reported that the NF-κB pathway regulates LPS-induced expression of IL-6, IL-12, and TNF-α,[36,37] and Saklatvala et al reported that MAPK activation is associated with enhanced production of TNF-α.[38] Taken together with our data, it is suggested that inhibition of both NF-κB and MAPK activation by tacrolimus leads to inhibition of the production of various cytokines by macrophages.

Another important finding in this study is that, in addition to inhibition of proinflammatory cytokine production, tacrolimus directly induced apoptosis of macrophages in vitro, and this in vitro effect was confirmed in our in vivo study, as shown by the increase of apoptotic macrophages in the colonic mucosa of IL-10-KO mice by rectal administration of tacrolimus. It is well known that tacrolimus strongly induces apoptosis of $CD4^+$ T cells.[39] In this study, we observed apoptosis of not only T cells but also macrophages in IL-10-KO mice. Thus, tacrolimus appears to induce apoptosis in both macrophages and T cells. We also observed in this study that the apoptotic effect of tacrolimus on macrophages is associated with caspase 3 and 9 activation. This result is consistent with previous data that tacrolimus enhances T-cell apoptosis through the activation of caspase 3.[39,40] In addition to caspase signaling, our data demonstrated that tacrolimus directly inhibits NF-κB activation in macrophages. Several reports have suggested that NF-κB activation is involved in the inhibition of apoptosis.[41,42] Thus, inhibition of NF-κB activation by tacrolimus may have roles not only in the suppression of proinflammatory cytokine production, but also in the induction of apoptosis in macrophages.

Finally, to confirm that tacrolimus ameliorates colonic inflammation through the inhibition of macrophages, we performed an in vivo study. We first evaluated the effects of tacrolimus in immune-mediated colitis of IL-10-KO mice, which mimic well the immune-mediated chronic

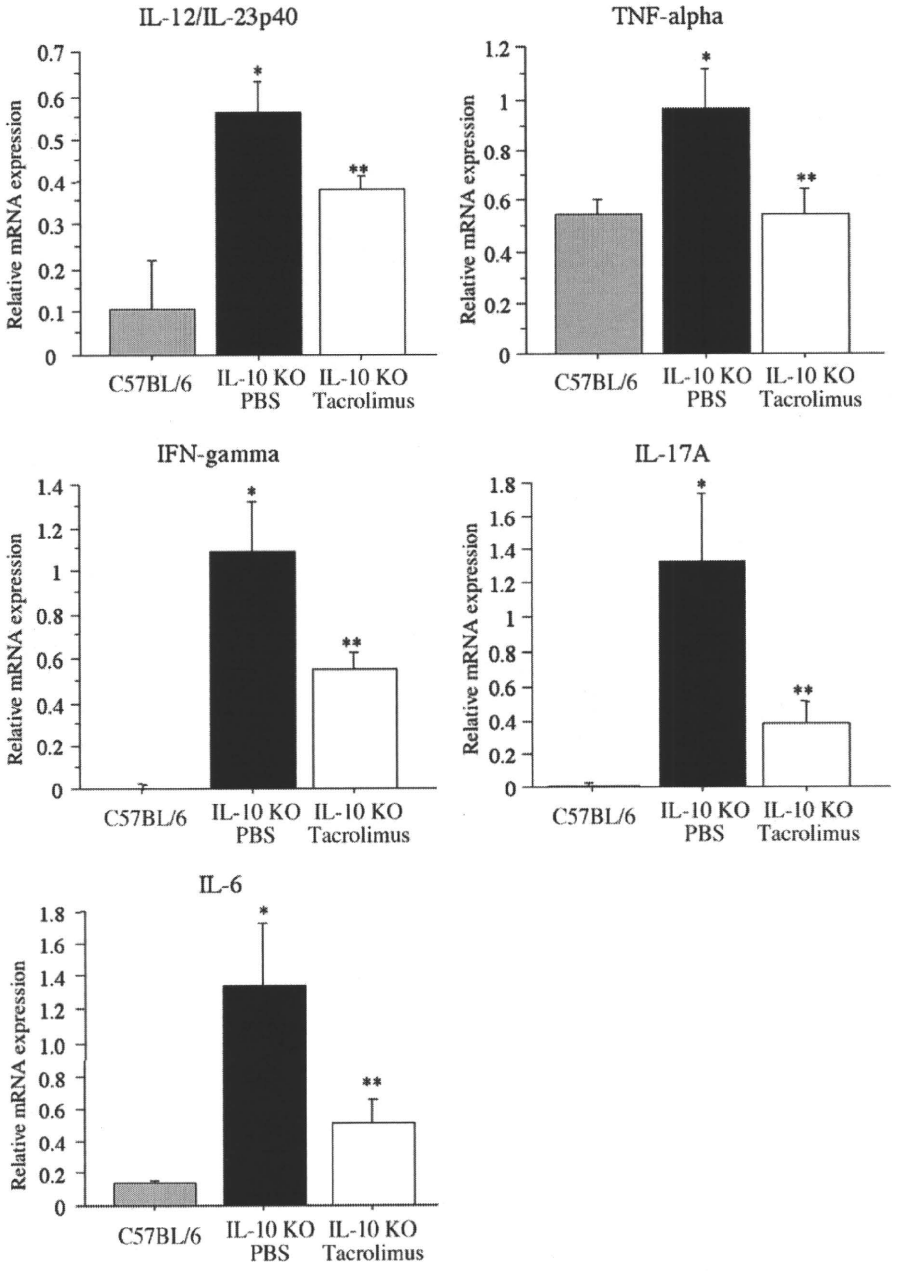

FIGURE 7. Effects of rectal administration of tacrolimus on transcript levels of IL-12/IL-23p40, TNF-α, IFN-γ, IL-17A, and IL-6 in colonic tissues of IL-10-KO mice in the therapeutic study. The gene expression of each target molecule was determined by semiquantitative PCR and was standardized against β-actin. Data are expressed as the mean ± SD (C57BL/6 mice, $n = 3$; IL-10-KO mice, $n = 7$ in each group); $^{*}P < 0.05$ compared with C57BL/6 mice, $^{**}P < 0.05$ compared with IL-10-KO mice without rectal administration of tacrolimus (PBS alone).

colonic inflammation observed in human IBD.[43] Our data clearly demonstrated that tacrolimus significantly improves colonic inflammation in IL-10-KO mice, and this is associated with apoptosis of macrophages in the colonic mucosa. Furthermore, we examined the effects of tacrolimus on DSS-induced colitis in CB.17/SCID mice. Because CB.17/SCID mice lack lymphocytes, T-cell-immune responses are not involved in the development of DSS-induced colitis in

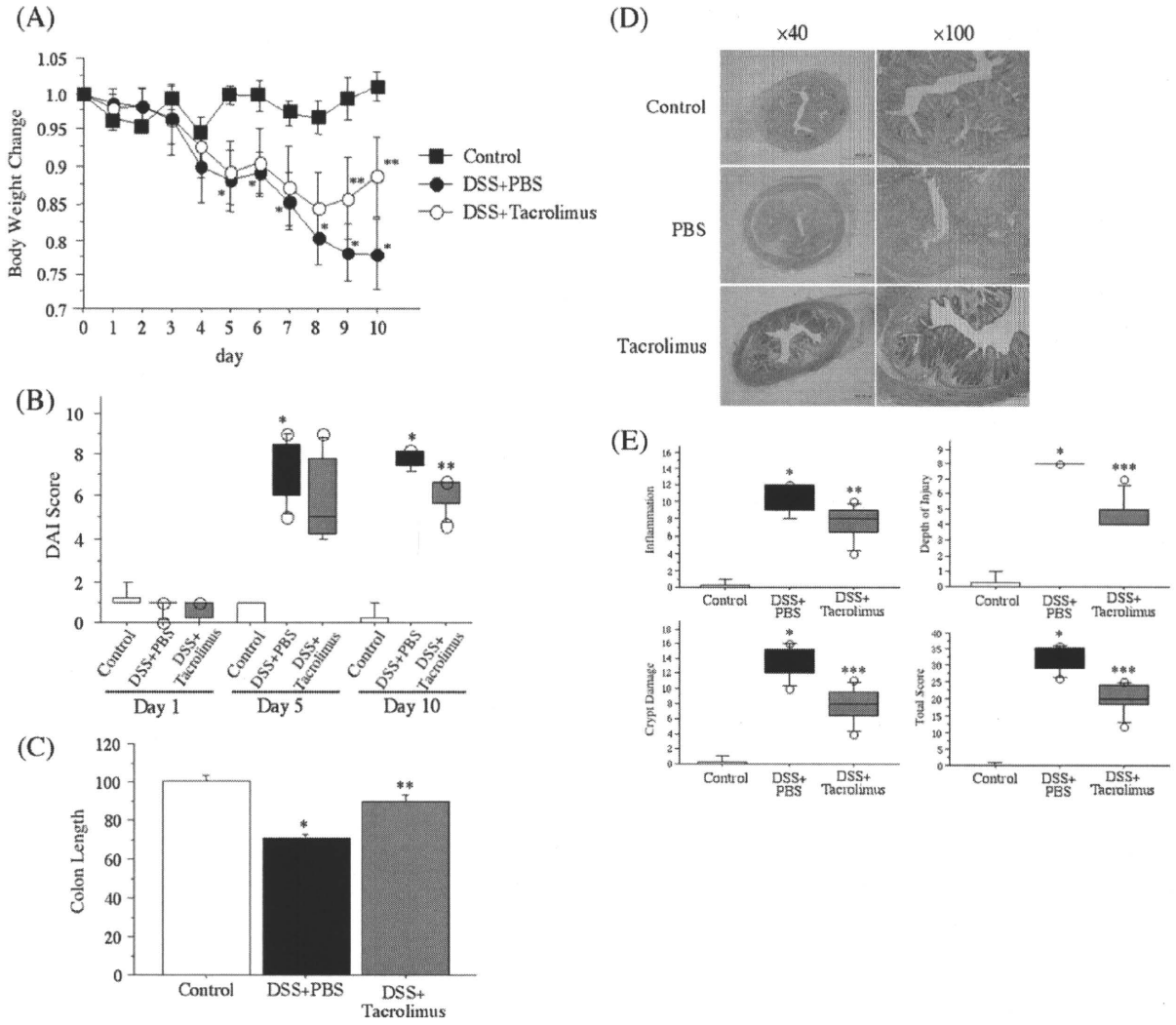

FIGURE 8. Therapeutic effects of tacrolimus on DSS-induced colitis in CB.17/SCID mice. A: Effects of rectal administration of tacrolimus on body weight changes. Serial changes in body weight were measured. Data are expressed as the mean ± SD (control group, $n = 5$; PBS group, $n = 8$; tacrolimus group, $n = 8$); $^{*}P < 0.05$ compared with control group (without DSS), $^{**}P < 0.05$ compared with PBS group (without tacrolimus). B: DAI score of DSS-induced colitis in CB.17/SCID mice treated with tacrolimus or PBS. Data are expressed as the mean ± SD (control group, $n = 5$; PBS group, $n = 8$; tacrolimus group, $n = 8$); $^{*}P < 0.001$ compared with control group (without DSS), $^{**}P < 0.05$ compared with PBS group (without tacrolimus). C: Effect of rectal administration of tacrolimus on colon length. Colon length was measured from the ileocecal junction to the anal verge. Data are expressed as the mean ± SD (control group, $n = 5$; PBS group, $n = 8$; tacrolimus group, $n = 8$); $^{*}P < 0.001$ compared with control group (without DSS), $^{**}P < 0.001$ compared with PBS group (without tacrolimus). D: Representative histological findings of mice treated with rectal administration of tacrolimus or PBS (original magnification 40× and 100×). E: Histological scores of colonic tissues in mice treated with rectal administration of tacrolimus or PBS. Data are expressed as the mean ± SD (control group, $n = 5$; PBS group, $n = 8$; tacrolimus group, $n = 8$); $^{*}P < 0.001$ compared with control group (without DSS), $^{**}P < 0.05$ and $^{***}P < 0.001$ compared with PBS group (without tacrolimus).

these mice. Interestingly, we found that tacrolimus ameliorated DSS-induced colitis in CB.17/SCID mice. These data strongly suggested that inhibitory effects of tacrolimus on macrophages contribute to amelioration of colonic inflammation.

In conclusion, our results confirmed the potential immunosuppressive effects of tacrolimus on activated macrophages. These inhibitory effects of tacrolimus on macrophages appear to play important roles in the treatment of colonic inflammation in patients with IBD.

REFERENCES

1. Calkins BM, Mendeloff AI. Epidemiology of inflammatory bowel disease. *Epidemiol Rev.* 1986;8:60–91.
2. Timmer A. Environmental influences on inflammatory bowel disease manifestations. Lessons from epidemiology. *Dig Dis.* 2003;21:91–104.
3. Sandborn WJ. Current directions in IBD therapy: what goals are feasible with biological modifiers? *Gastroenterology.* 2008;135: 1442–1447.
4. Sartor RB. Current concepts of the etiology and pathogenesis of ulcerative colitis and Crohn's disease. *Gastroenterol Clin North Am.* 1995; 24:475–507.
5. Cario E, Podolsky DK. Differential alteration in intestinal epithelial cell expression of toll-like receptor 3 (TLR3) and TLR4 in inflammatory bowel disease. *Infect Immun.* 2000;68:7010–7017.
6. Kucharzik T, Maaser C, Lugering A, et al. Recent understanding of IBD pathogenesis: implications for future therapies. *Inflamm Bowel Dis.* 2006;12:1068–1083.
7. Watanabe T, Kitani A, Murray PJ, et al. NOD2 is a negative regulator of Toll-like receptor 2-mediated T helper type 1 responses. *Nat Immunol.* 2004;5:800–808.
8. Massey DC, Parkes M. Genome-wide association scanning highlights two autophagy genes, ATG16L1 and IRGM, as being significantly associated with Crohn's disease. *Autophagy.* 2007;3:649–651.
9. Henckaerts L, Figueroa C, Vermeire S, et al. The role of genetics in inflammatory bowel disease. *Curr Drug Targets.* 2008;9:361–368.
10. Kaisho T, Akira S. Toll-like receptors and their signaling mechanism in innate immunity. *Acta Odontol Scand.* 2001;59:124–130.
11. Schenk M, Mueller C. Adaptations of intestinal macrophages to an antigen-rich environment. *Semin Immunol.* 2007;19:84–93.
12. Kamada N, Hisamatsu T, Okamoto S, et al. Unique CD14 intestinal macrophages contribute to the pathogenesis of Crohn disease via IL-23/IFN-gamma axis. *J Clin Invest.* 2008;118:2269–2280.
13. Nakase H, Okazaki K, Tabata Y, et al. Development of an oral drug delivery system targeting immune-regulating cells in experimental inflammatory bowel disease: a new therapeutic strategy. *J Pharmacol Exp Ther.* 2000;292:15–21.
14. Kanai T, Uraushihara K, Totsuka T, et al. Ameliorating effect of saporin-conjugated anti-CD11b monoclonal antibody in a murine T-cell-mediated chronic colitis. *J Gastroenterol Hepatol.* 2006;21:1136–1142.
15. Sawada S, Suzuki G, Kawase Y, et al. Novel immunosuppressive agent, FK506. In vitro effects on the cloned T cell activation. *J Immunol.* 1987;139:1797–1803.
16. Schreiber SL. Chemistry and biology of the immunophilins and their immunosuppressive ligands. *Science.* 1991;251:283–287.
17. Liu J, Farmer JD, Jr., Lane WS, et al. Calcineurin is a common target of cyclophilin-cyclosporin A and FKBP-FK506 complexes. *Cell.* 1991;66:807–815.
18. Schreiber SL, Crabtree GR. The mechanism of action of cyclosporin A and FK506. *Immunol Today.* 1992;13:136–142.
19. Todo S, Fung JJ, Starzl TE, et al. Liver, kidney, and thoracic organ transplantation under FK 506. *Ann Surg.* 1990;212:295–305; discussion 306–297.
20. Baumgart DC, Pintoffl JP, Sturm A, et al. Tacrolimus is safe and effective in patients with severe steroid-refractory or steroid-dependent inflammatory bowel disease—a long-term follow-up. *Am J Gastroenterol.* 2006;101:1048–1056.
21. Qualls JE, Kaplan AM, van Rooijen N, et al. Suppression of experimental colitis by intestinal mononuclear phagocytes. *J Leukoc Biol.* 2006;80:802–815.
22. O'Mahony L, Feeney M, O'Halloran S, et al. Probiotic impact on microbial flora, inflammation and tumour development in IL-10 knockout mice. *Aliment Pharmacol Ther.* 2001;15:1219–1225.
23. Cooper HS, Murthy SN, Shah RS, et al. Clinicopathologic study of dextran sulfate sodium experimental murine colitis. *Lab Invest.* 1993; 69:238–249.
24. Vowinkel T, Kalogeris TJ, Mori M, et al. Impact of dextran sulfate sodium load on the severity of inflammation in experimental colitis. *Dig Dis Sci.* 2004;49:556–564.
25. Kamada N, Hisamatsu T, Okamoto S, et al. Abnormally differentiated subsets of intestinal macrophage play a key role in Th1-dominant chronic colitis through excess production of IL-12 and IL-23 in response to bacteria. *J Immunol.* 2005;175:6900–6908.
26. Bettelli E, Kuchroo VK. IL-12- and IL-23-induced T helper cell subsets: birds of the same feather flock together. *J Exp Med.* 2005;201:169–171.
27. Dong C. Diversification of T-helper-cell lineages: finding the family root of IL-17-producing cells. *Nat Rev Immunol.* 2006;6:329– 333.
28. Oppmann B, Lesley R, Blom B, et al. Novel p19 protein engages IL-12p40 to form a cytokine, IL-23, with biological activities similar as well as distinct from IL-12. *Immunity.* 2000;13:715–725.
29. Yang J, Murphy TL, Ouyang W, et al. Induction of interferon-gamma production in Th1 CD4+ T cells: evidence for two distinct pathways for promoter activation. *Eur J Immunol.* 1999;29:548–555.
30. Langrish CL, Chen Y, Blumenschein WM, et al. IL-23 drives a pathogenic T cell population that induces autoimmune inflammation. *J Exp Med.* 2005;201:233–240.
31. Hsieh CS, Macatonia SE, Tripp CS, et al. Development of TH1 CD4+ T cells through IL-12 produced by Listeria-induced macrophages. *Science.* 1993;260:547–549.
32. Fujino S, Andoh A, Bamba S, et al. Increased expression of interleukin 17 in inflammatory bowel disease. *Gut.* 2003;52:65–70.
33. Lan CC, Yu HS, Wu CS, et al. FK506 inhibits tumour necrosis factor-alpha secretion in human keratinocytes via regulation of nuclear factor-kappaB. *Br J Dermatol.* 2005;153:725–732.
34. Diestel A, Roessler J, Pohl-Schickinger A, et al. Specific p38 inhibition in stimulated endothelial cells: a possible new anti-inflammatory strategy after hypothermia and rewarming. *Vascul Pharmacol.* 2009; 51:246–252.
35. Barton GM, Medzhitov R. Toll-like receptor signaling pathways. *Science.* 2003;300:1524–1525.
36. Neurath MF, Fuss I, Schurmann G, et al. Cytokine gene transcription by NF-kappa B family members in patients with inflammatory bowel disease. *Ann N Y Acad Sci.* 1998;859:149–159.
37. Zhang JS, Feng WG, Li CL, et al. NF-kappa B regulates the LPS-induced expression of interleukin 12 p40 in murine peritoneal macrophages: roles of PKC, PKA, ERK, p38 MAPK, and proteasome. *Cell Immunol.* 2000;204:38–45.
38. Saklatvala J. The p38 MAP kinase pathway as a therapeutic target in inflammatory disease. *Curr Opin Pharmacol.* 2004;4:372–377.
39. Choi SJ, You HS, Chung SY. Tacrolimus-induced apoptotic signal transduction pathway. *Transplant Proc.* 2008;40:2734–2736.
40. Hortelano S, Lopez-Collazo E, Bosca L. Protective effect of cyclosporin A and FK506 from nitric oxide-dependent apoptosis in activated macrophages. *Br J Pharmacol.* 1999;126:1139–1146.
41. Van Antwerp DJ, Martin SJ, Kafri T, et al. Suppression of TNF-alpha-induced apoptosis by NF-kappaB. *Science.* 1996;274:787–789.
42. Beg AA, Baltimore D. An essential role for NF-kappaB in preventing TNF-alpha-induced cell death. *Science.* 1996;274:782–784.
43. Kuhn R, Lohler J, Rennick D, et al. Interleukin-10-deficient mice develop chronic enterocolitis. *Cell.* 1993;75:263–227.

The Journal of Nutrition
Biochemical, Molecular, and Genetic Mechanisms

Identification and Comparative Functional Characterization of a New Human Riboflavin Transporter hRFT3 Expressed in the Brain[1–3]

Yoshiaki Yao, Atsushi Yonezawa, Hiroki Yoshimatsu, Satohiro Masuda, Toshiya Katsura and Ken-ichi Inui*

Department of Pharmacy, Kyoto University Hospital, Faculty of Medicine, Sakyo-ku, Kyoto 606-8507, Japan

Abstract

We isolated cDNA coding a new human riboflavin transporter (hRFT)3, which exhibits 86.7 and 44.1% amino acid identity with hRFT1 and hRFT2, respectively. It was predicted to have 10 putative membrane-spanning domains. The functional characteristics of hRFT3 were examined and compared with those of its isoforms, hRFT1 and hRFT2. Real-time PCR revealed that hRFT3 mRNA was strongly expressed in the brain and salivary gland. hRFT1 mRNA was strongly expressed in the placenta and small intestine, whereas hRFT2 mRNA was most abundantly expressed in the testis and strongly in the small intestine and prostate. hRFT-mediated uptake of [^{3}H]riboflavin was evaluated using human embryonic kidney 293 cells transiently transfected with the cDNA coding each hRFT. The apparent Michaelis-Menten constants of hRFT1, hRFT2, and hRFT3 for riboflavin were 1.38, 0.98, and 0.33 μmol/L, respectively. The hRFT-mediated [^{3}H]riboflavin uptake was independent of extracellular Na^+ and Cl^-. Specific uptake of [^{3}H]riboflavin by hRFT2, but not hRFT1 and hRFT3, decreased as extracellular pH was changed from 5.4 to 8.4. The substrate specificities of the hRFT family were similar. hRFT-mediated uptake of [^{3}H]riboflavin was inhibited by some riboflavin analogs, but not D-ribose, organic ions, or other vitamins. The newly isolated hRFT3 may play an important role in brain riboflavin homeostasis. Its amino acid sequence and functional characteristics are similar to those of hRFT1, but not hRFT2. J. Nutr. 140: 1220–1226, 2010.

Introduction

The water-soluble vitamin riboflavin is essential for normal cellular functions. It is converted to the coenzyme forms flavin mononucleotide (FMN) and flavin adenine dinucleotide (FAD) by flavokinases and FAD synthases. These flavins participate in cellular metabolic reactions as intermediaries in biochemical oxidation-reduction reactions, including carbohydrate, lipid, and amino acid metabolism (1). Humans are unable to synthesize riboflavin and therefore must obtain it via intestinal absorption. Over the last 5 decades, many studies using intestinal specimens, intestinal membrane vesicles, and cell lines have indicated that absorption of riboflavin in the intestine is mediated by transporter(s) (2).

Recently, we identified novel human riboflavin transporter (hRFT)1[4] and rat riboflavin transporter (rRFT)1 using our rat kidney mRNA expression database (3). hRFT1 was originally annotated as G protein-coupled receptor (GPR) 172B (GenBank accession no. NM_017986.2), but its molecular function had yet to be determined. It was predicted to have 10 putative membrane-spanning domains by the SOSUI program (4) and, thus, this protein was postulated to be a transporter rather than a receptor. Screening for its substrate(s) was carried out using the small interfering RNA approach, because it was endogenously expressed in various cultured cells. We found that riboflavin is a specifically transported substrate for it and renamed it hRFT1. It exhibits no similarity to a bacterial riboflavin transporter RibU or impX (5,6), a yeast riboflavin transporter Mch5p (7), or any other mammalian transporters. Riboflavin transporter (RFT)1 is

[1] Supported in part by a grant-in-aid for Scientific Research (KAKENHI) from the Ministry of Education, Science, Culture and Sports of Japan.
[2] Author disclosures: Y. Yao, A. Yonezawa, H. Yoshimatsu, S. Masuda, T. Katsura, and K. Inui, no conflicts of interest.
[3] Supplemental Figures 1 and 2 are available with the online posting of this paper at jn.nutrition.org.
* To whom correspondence should be addressed. E-mail: inui@kuhp.kyoto-u.ac.jp.

[4] Abbreviations used: EGFP, enhanced green fluorescent protein; FAD, flavin adenine dinucleotide; FMN, flavin mononucleotide; GPR, G protein-coupled receptor; HEK, human embryonic kidney; hRFT, human riboflavin transporter; K_m, Michaelis-Menten constant; RFT, riboflavin transporter; rRFT, rat riboflavin transporter; V_{max}, maximal transport rate.

Manuscript received February 18, 2010. Initial review completed March 22, 2010. Revision accepted April 13, 2010.
First published online May 12, 2010; doi:10.3945/jn.110.122911.

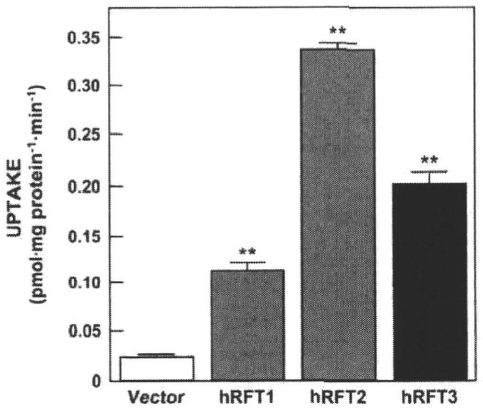

FIGURE 1 Uptake of [^{3}H]riboflavin by HEK293 cells transfected with empty vector, hRFT1, hRFT2, and hRFT3. The cells were incubated in buffer (pH 7.4) containing 5 nmol/L [^{3}H]riboflavin for 1 min at 37°C. Each bar represents the mean ± SEM, n = 3. **Different from vector-transfected cells, $P < 0.01$.

therefore indicated to be the first member of a novel mammalian riboflavin transporter RFT family.

Thereafter, the second member RFT2 was also identified as a homolog of RFT1 (8). hRFT2 shows 42.9% amino acid identity with hRFT1. hRFT1 mRNA was strongly expressed in the placenta and small intestine, whereas rRFT2 mRNA was strongly expressed in the testis and small intestine (3,8). Based on these results, RFT1 and RFT2 were suggested to play important roles in intestinal riboflavin absorption. After absorption, riboflavin is distributed from the blood to several tissues and utilized as a coenzyme in metabolic reactions. Yet in some tissues, such as brain and liver, RFT1 and RFT2 were only slightly expressed. Therefore, another member belonging to the RFT family could play a key role in riboflavin handling.

In this study, we successfully isolated hRFT3 as a new member of the RFT gene family. hRFT3 mRNA was strongly expressed in the brain. Because the functional characteristics of hRFT1 and hRFT2 had not been clearly demonstrated, we compared functional characteristics of hRFT3 with those of hRFT1 and hRFT2.

Materials and Methods

Isolation of hRFT3. We searched for the human homolog of hRFT1 in the GenBank database by using the BLASTN algorithm and found GPR 172A (GenBank accession no. NM_024531) as well as hRFT2. The molecular function of GPR172A has yet to be determined. We designated it hRFT3 (GenBank accession no. AB522904) based on its functional characterization as shown below. In addition, we also searched for the rat ortholog, but no clone was identified except for rRFT1 and rRFT2. The hRFT3 cDNA was isolated by RT-PCR with the forward primer 5′-GGAAGCTTGCCCTAGGTGGGAAAAGAAC-3′ and the reverse primer 5′-GGTCTAGAGAGGGAAAGACAGGTGTTGG-3′ using human small intestine-derived total RNA commercially purchased from Clontech. The PCR was performed using PrimeSTAR HS DNA Polymerase (TAKARA BIO) according to the following profile: 98°C for 10 s, 52°C for 5 s, 72°C for 2.5 min, 36 cycles. The hRFT2 cDNA was isolated similarly using hRFT2-specific primers designed based on the sequence in GenBank (accession no. NM_033409). The primers were as follows: forward primer 5′-GGAAGCTTCAGTCCAGATCCCAGGAGAG-3′ and reverse primer 5′-GGCTCGAGGGAGATCTGAGCTGGTCGTC-3′. PCR products were subcloned into the expression vector pcDNA3.1/Hygro(+) (Life Technologies) or pEnhanced Green Fluorescent Protein (EGFP)-C1 (Clontech) and sequenced using a 96-capillary 3730xl DNA Analyzer (Life Technologies).

The hRFT1 cDNA was previously isolated and subcloned into the expression vector pBK-CMV (Stratagene) (3). It was amplified by PCR with the hRFT1 plasmid using hRFT1-specific following primers designed based on the sequence in GenBank (accession no. AB362533): forward primer 5′-GGAAGCTTTTCCAGAAGAGCCAAAGCAT-3′ and reverse primer 5′-GGTCTAGAGCCTCACGATGAAGACAGGT-3′ and it was subcloned into the expression vector pcDNA3.1/Hygro(+) or pEGFP-C1. Multiple sequence alignments and phylogenic trees were produced using GENETYX-MAC version 13 (Software Development).

Cell culture and transfection. Human embryonic kidney (HEK)293 cells (American Type Culture Collection CRL-1573) were cultured in the complete medium consisting of DMEM (Wako Pure Chemical Industries) supplemented with 10% fetal bovine serum (Life Technologies) in an atmosphere of 5% CO_2-95% air at 37°C.

For a transient expression system, pcDNA3.1/Hygro(+) and pEGFP-C1 containing hRFT1, hRFT2, and hRFT3 were purified using the Hispeed Plasmid Purification system (QIAGEN K.K) and Wizard Plus SV Minipreps DNA Purification system (Promega), respectively. On the day before transfection, cells were seeded onto poly-D-lysine–coated 24-well plates (Becton, Dickinson and Company) at a density of 7.5×10^4 cells/well for the uptake experiment, poly-D-lysine/laminin–coated 4-well culture slide (Becton, Dickinson and Company) at a density of 2.0×10^5

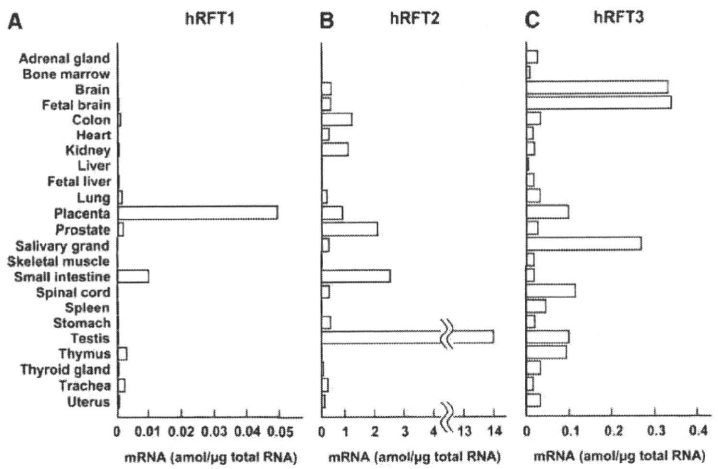

FIGURE 2 Real-time PCR analysis of various human tissues for hRFT1 (*A*), hRFT2 (*B*), and hRFT3 (*C*). Total RNA of various human tissues was reverse-transcribed to yield cDNA.

cells/well for fluorescence chemistry, and 60-mm tissue culture dish (Asahi Glass) at a density of 2.0×10^6 cells/dish for Western blot analysis. The cells were transfected with 0.2 μg of plasmid DNA using 1 μL of Lipofectamine 2000 Reagent (Life Technologies) per well for the uptake experiment, 0.8 μg of plasmid DNA using 2 μL of Lipofectamine 2000 Reagent per well for fluorescence chemistry, and 8 μg of plasmid DNA using 20 μL of Lipofectamine 2000 Reagent for Western blot analysis according to the manufacturer's instructions. Forty-eight hours after transfection, the cells were used for subsequent experiments.

Real-time PCR. Total RNA (1 μg) from various human tissues was commercially purchased from Clontech and reverse-transcribed to yield cDNA. To determine the sum of the mRNA expression of hRFT1, hRFT2, and hRFT3, real-time PCR was performed with an ABI PRISM 7700 sequence detector (Life Technologies). Real-time PCR was carried out in a total volume of 20 μL containing 5 μL of cDNA sample, 2 μL of TaqMan Gene Expression assays, and 10 μL of TaqMan Universal Master mix (Life Technologies). The starting mRNA copy number of the target sequence was established by determining the fractional PCR threshold cycle number at which a fluorescence signal generated during the replication process passed above a threshold value. The initial amount of target mRNA in each sample was estimated from the experimental threshold cycle value with a standard curve generated using known amounts of standard plasmid DNA. Real-time PCR conditions were as follows: 95°C for 15 s, 60°C for 60 s, 50 cycles. TaqMan Gene Expression assays were purchased from Life Technologies: hRFT1, Hs01079030_gl; hRFT2, Hs00364295_ml; hRFT3, Hs01859203_sl.

Fluorescence cytochemistry. HEK293 cells were transfected with the plasmid vector pEGFP-C1 containing hRFT1, hRFT2, and hRFT3 as described above. The cells were fixed with 2% paraformaldehyde for 10 min at room temperature and observed using a BIOREVO BZ-9000 fluorescence microscope (KEYENCE).

Western blot analysis. Western blot analysis was carried out using a NuPAGE electrophoresis system (Life Technologies) as described previously with some modifications (9). Briefly, cells were homogenized by sonication in buffer (250 mmol/L sucrose and 5 mmol/L HEPES, pH 7.4) and were then centrifuged at 2000 × *g* for 10 min. The supernatant was recentrifuged at 15,000 × g for 30 min and the pellet was used for the crude membrane samples. Crude membrane fractions (2.5 μg) were separated by NuPAGE 4–12% Bis-Tris gels, 1.0 mm, 12 well (Life Technologies), and were transferred onto 0.2 μm polyvinylidene difluoride membrane (Life Technologies) according to the manufacturer's instructions. Primary and secondary antibodies were anti-green fluorescent protein (Roche Diagnostics) and horseradish peroxidase-conjugated anti-mouse IgG (GE Healthcare Bio-Sciences), respectively. The bound antibody was detected on X-ray film using a Visualizer Spray and Glow ECL Western Blotting system (Millipore).

Uptake experiment. Cellular uptake of [^{3}H]riboflavin (0.903 TBq/mmol, Moravek Biochemicals) was measured with monolayer cultures grown on poly-D-lysine–coated 24-well plates. The experimental procedures were described previously (3,10). Briefly, the cells were preincubated with 0.2 mL of incubation buffer (pH 7.4) for 10 min at 37°C. The buffer was then removed and 0.2 mL of each incubation buffer containing 5 nmol/L [^{3}H] riboflavin was added. The buffer was aspirated at the end of the incubation period and the monolayers were rapidly washed twice with 1 mL of ice-cold incubation buffer. The cells were solubilized in 0.5 mL of 0.5 mol/L NaOH and then the radioactivity in aliquots was determined by liquid scintillation counting. The composition of incubation buffer was as follows: 145 mmol/L NaCl, 3 mmol/L KCl, 1 mmol/L $CaCl_2$, 0.5 mmol/L $MgCl_2$, 5 mmol/L D-glucose, and 5 mmol/L HEPES (pH 7.4 unless otherwise specified; pH was adjusted with NaOH). Na^+-free incubation buffer was prepared by replacing Na^+ with N-methyl-D-glucamine or choline (pH 7.4; pH was adjusted with HCl or KOH), and Cl^--free incubation buffer was prepared by replacing Cl^- with gluconate or sulfate (pH 7.4; pH was adjusted with NaOH). The protein content of the solubilized cells was determined by the method of Bradford with a Bio-Rad Protein Assay kit (Bio-Rad Laboratories) with bovine γ-globulin as a standard.

The specific uptake of [^{3}H]riboflavin by hRFT1, hRFT2, and hRFT3 was calculated by subtracting the uptake of [^{3}H]riboflavin by HEK293 cells transfected with empty vector from uptake with each hRFT. The concentration dependence of riboflavin transport was fit by the Michaelis-Menten equation: $V = V_{max}[S]/(K_m + [S])$, where V is the transport rate, V_{max} is the maximal transport rate, [S] is the concentration of riboflavin, and K_m is the Michaelis-Menten constant.

Statistical analysis. Data are expressed as the means ± SEM. Time dependence or concentration dependence of riboflavin transport was analyzed by 1-way ANOVA using GraphPad Prism (version 5.0b, GraphPad Software). Other data were analyzed by Dunnett's 2-tailed test after 1-way ANOVA. $P < 0.05$ was considered significant.

Results

Isolation of a new hRFT3. A single clone encoding hRFT3 was isolated and sequenced. The hRFT3 cDNA (GenBank accession no. AB522904) consists of 1451 bp with an open reading frame encoding a 445-amino acid protein. It was predicted to have 10 putative membrane-spanning domains by the SOSUI program

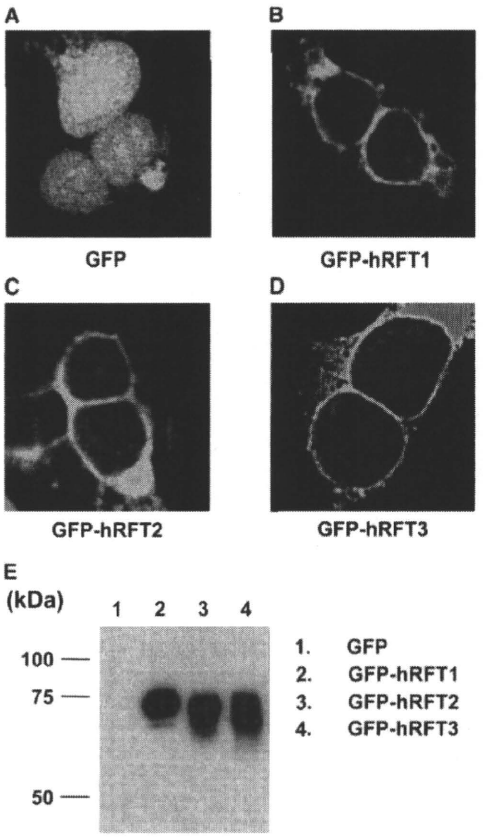

FIGURE 3 Fluorescence cytochemistry (*A–D*) and Western blotting (*E*) of EGFP-tagged empty vector, hRFT1, hRFT2, and hRFT3 introduced in HEK293 cells. Cells were fixed with 2% paraformaldehyde and observed using BIOREVO BZ-9000 fluorescence microscope. Western blot analysis was performed using the crude membrane of HEK293 cells expressing EGFP-tagged hRFT1, hRFT2, and hRFT3.

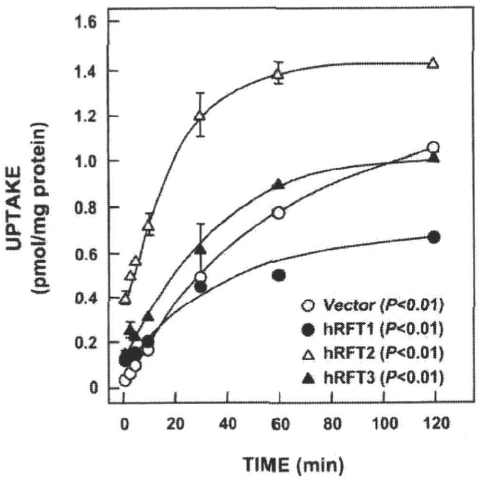

FIGURE 4 Time-dependent uptake of [^{3}H]riboflavin by HEK293 cells transfected with empty vector, hRFT1, hRFT2, and hRFT3. The cells were incubated in incubation buffer (pH 7.4) containing 5 nmol/L [^{3}H] riboflavin for various periods at 37°C. Each point represents the mean ± SEM, n = 3.

(4). hRFT3 shows 86.7% amino acid identity with hRFT1, 81.5% with rRFT1, 44.1% with hRFT2, and 43.1% with rRFT2. The amino acid sequences and phylogenic trees of hRFT3, hRFT1, rRFT1, hRFT2, and rRFT2 are shown in **Supplemental Figure 1**. The uptake of [^{3}H]riboflavin was significantly increased by transfection with hRFT3 as well as hRFT1 and hRFT2 (**Fig. 1**), indicating that hRFT3 is also a riboflavin transporter of the RFT family.

Tissue distribution and cellular localization of hRFT1, hRFT2, and hRFT3. The mRNA levels of hRFT1, hRFT2, and hRFT3 were examined by real-time PCR (**Fig. 2**). The hRFT1 mRNA was expressed in the placenta and small intestine. hRFT2 was primarily expressed in the testis and strongly in the small intestine and prostate. hRFT3 was strongly expressed in the brain, fetal brain, and salivary gland. To visualize the cellular localization of these proteins, EGFP-tagged hRFT1, hRFT2, and hRFT3 was introduced into HEK293 cells. Fluorescence was observed in the plasma membrane of the cells transfected with EGFP-tagged hRFT1, hRFT2, and hRFT3 (**Fig. 3***B–D*). In addition, Western blot analysis was carried out using the crude membrane of HEK293 cells transfected with these cDNA (Fig. 3*E*). A strong signal for EGFP-tagged hRFT1, hRFT2, and hRFT3 was detected.

Functional characterization of hRFT1, hRFT2, and hRFT3. We examined the uptake of [^{3}H]riboflavin by HEK293 cells transfected with empty vector, hRFT1, hRFT2, and hRFT3. The uptake of [^{3}H]riboflavin increased in a time-dependent manner (**Fig. 4**) and in a concentration-dependent manner (**Fig. 5***A*). The specific uptake by each hRFT was calculated (Fig. 5*B–D*). In addition, Eadie-Hofstee plots were constructed (Fig. 5*E–G*). The apparent K_m values of hRFT1, hRFT2, and hRFT3 for riboflavin were 1.38 ± 0.27, 0.98 ± 0.11, and 0.33 ± 0.07 μmol/L, respectively, and V_{max} values of these transporters were 12.2 ± 0.8, 63.8 ± 9.3, and 5.2 ± 0.7 pmol·mg protein^{-1}·min^{-1}, respectively. The replacement of Na^+ with N-methyl-D-glucamine or choline did not affect hRFT-mediated uptake of [^{3}H]riboflavin

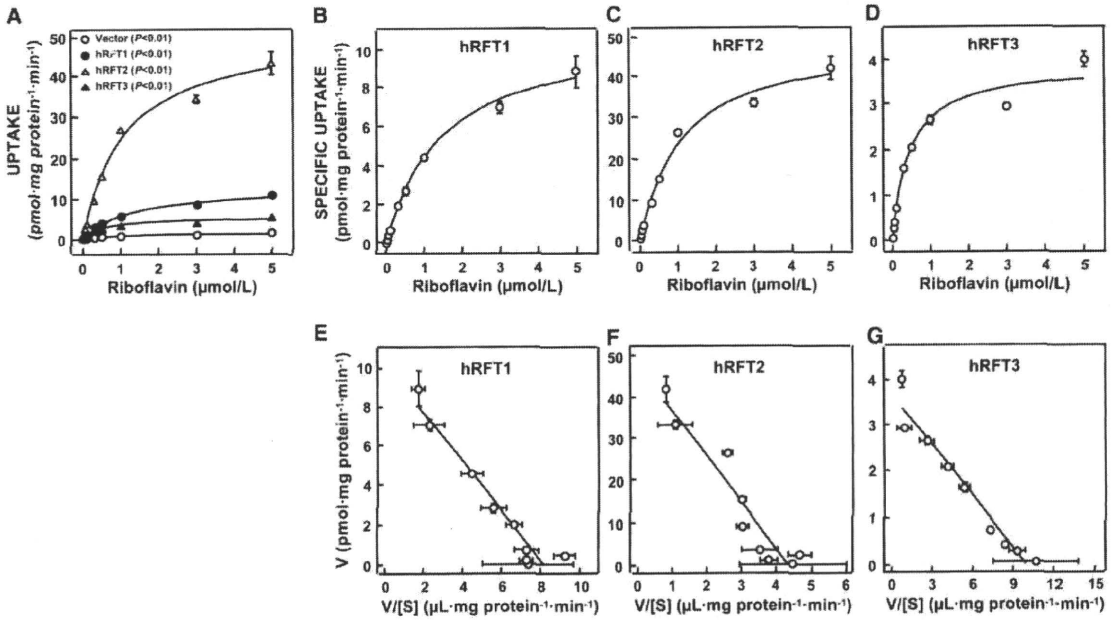

FIGURE 5 Concentration-dependent uptake of [^{3}H]riboflavin by HEK293 cells transfected with empty vector, hRFT1, hRFT2, and hRFT3 (*A*). The specific uptake of [^{3}H]riboflavin by hRFT1 (*B*), hRFT2 (*C*), and hRFT3 (*D*) was calculated by subtracting the uptake of [^{3}H]riboflavin by HEK293 cells transfected with empty vector from the uptake with hRFT. Eadie-Hofstee plots of the concentration-dependent uptake by each hRFT (*E–G*) are shown. The cells were incubated in buffer (pH 7.4) containing [^{3}H]riboflavin at various concentrations for 1 min at 37°C. Each point represents the mean ± SEM, n = 3.

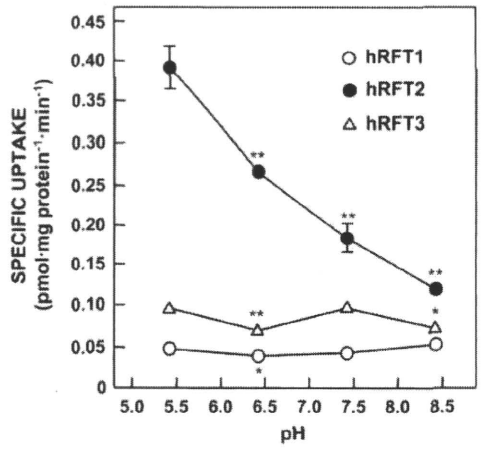

FIGURE 6 pH dependence of [^{3}H]riboflavin uptake by HEK293 cells transfected with hRFT1, hRFT2, and hRFT3. The specific uptake of [^{3}H]riboflavin by hRFT1, hRFT2, and hRFT3 was calculated by subtracting the uptake of [^{3}H]riboflavin by HEK293 cells transfected with empty vector from the uptake with hRFT family genes. The cells were incubated in buffer (pH 5.4–8.4) containing 5 nmol/L [^{3}H] riboflavin for 1 min at 37°C. Each point and bar represents the mean ± SEM, $n = 3$. Asterisks indicate different from cells incubated at pH 5.4: $^*P < 0.05$, $^{**}P < 0.01$.

(**Supplemental Fig. 2A**). Similarly, the replacement of Cl^- with gluconate or sulfate did not affect specific uptake by these transfectants (Supplemental Fig. 2*B*). We observed no pH dependence of hRFT1- and hRFT3-mediated uptake of [^{3}H] riboflavin (**Fig. 6**). The transport of [^{3}H]riboflavin by hRFT2, however, decreased as the extracellular pH was changed from 5.4 to 8.4. The chemical structures of riboflavin and its analogs are shown in **Figure 7A**. The hRFT1-, hRFT2-, and hRFT3-mediated uptakes of [^{3}H]riboflavin were completely inhibited by excess unlabeled riboflavin and lumiflavine, whereas they were modestly inhibited by FMN (Fig. 7*B–D*). FAD slightly but significantly inhibited the hRFT3-mediated uptake of [^{3}H]riboflavin. D-Ribose, cimetidine, probenecid, thiamine, and folate only slightly and in several instances not significantly affected the specific uptake of [^{3}H]riboflavin by hRFT1, hRFT2, and hRFT3.

Discussion

In the present study, we identified hRFT3, which is a new member of the RFT gene family. The deduced amino acid sequence of hRFT3 shows 86.7 and 44.1% identity with hRFT1 and hRFT2, respectively (Supplemental Fig. 1). Based on their amino acid sequences, hRFT3 and hRFT1 were originally annotated as GPR172A (GenBank accession no. NM_024531) and GPR172B (GenBank accession no. NM_017986.2), respectively. However, their functional characteristics as GPR have not been demonstrated. They were predicted to have 10 putative membrane-spanning domains by the SOSUI program (4) and their riboflavin transport activity was indicated (Figs. 1, 4, 5). These results indicated that the GPR172 family could be designated as riboflavin transporter RFT family.

Interestingly, hRFT3 mRNA was predominantly expressed in the brain, whereas hRFT1 and hRFT2 mRNA were strongly expressed in the small intestine, but not brain (Fig. 2). The brain has developed specific carrier systems for the uptake of vital nutrients (e.g. glucose, amino acids, vitamins, and minerals), which are independent of intestinal transporters involved in absorption of the nutrients. For example, facilitative glucose transporter 1, rather than intestinal glucose transporter 2, plays a role in glucose uptake in the brain (11–13). In addition, brain-type sodium-dependent vitamin C transporter 2, but not intestinal sodium-dependent vitamin C transporter 1, is important for ascorbic acid homeostasis (14,15). In the case of riboflavin, a carrier-mediated mechanism also maintains riboflavin homeostasis in the brain (16–19). Thus, there is much interest in how hRFT3 works in the brain.

Previous studies demonstrated that the concentration of total riboflavin (riboflavin, FMN, and FAD) in the brain was 8.8 μmol/L, which was ~50 times higher than in plasma in adult rabbits (16,17). In addition, the concentrations of FMN and FAD in the brain remained relatively constant in severe deficiency as well as after high doses of riboflavin (18). It was also reported that

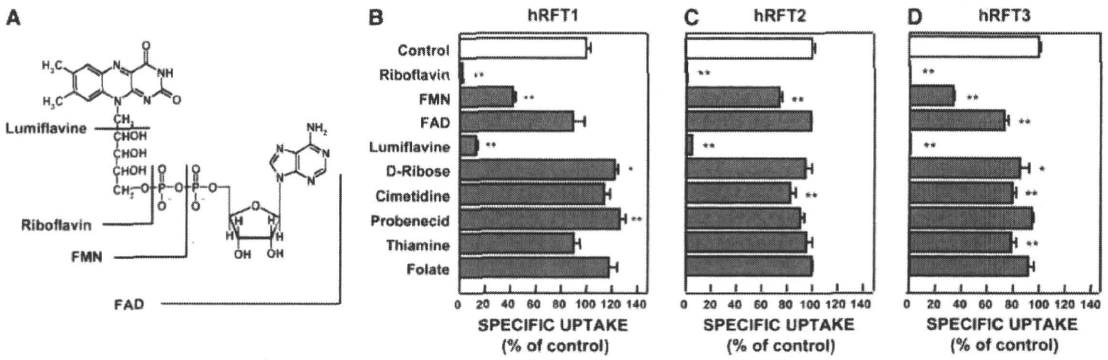

FIGURE 7 The chemical structure of riboflavin and its analogs (*A*) and the inhibitory effect of riboflavin analogs at 0.1 mmol/L and other inhibitors at 1.0 mmol/L on the specific uptake of [^{3}H]riboflavin by HEK293 cells transfected with hRFT1 (*B*), hRFT2 (*C*), and hRFT3 (*D*). The specific uptake of [^{3}H]riboflavin by hRFT1, hRFT2, and hRFT3 was calculated by subtracting the uptake of [^{3}H]riboflavin by HEK293 cells transfected with empty vector from the uptake with hRFT1, hRFT2, and hRFT3. The cells were incubated in buffer (pH 7.4) containing 5 nmol/L [^{3}H]riboflavin in the presence of inhibitors for 1 min at 37°C. Each bar represents the mean ± SEM, $n = 3$. Asterisks indicate different from control cells: $^*P < 0.05$, $^{**}P < 0.01$.

isolated rabbit brain slices contained a saturable accumulation system for riboflavin, which was inhibited by other flavins but not by D-ribose and probenecid (19). These previous reports indicated that the characteristics of riboflavin transport in the brain were similar to those of hRFT3 (Figs. 4, 5*D*, 7*D*). Therefore, hRFT3 would play an important role in the maintenance of riboflavin homeostasis in the brain.

Comparative functional characterization of hRFT1, hRFT2, and hRFT3 was carried out in this study and revealed some differences in the features of the hRFT family. hRFT1, hRFT2, and hRFT3 were independent of extracellular Na^+ and Cl^- (Supplemental Fig. 2*A*,*B*) and their substrate specificities were similar (Fig. 7*B*–*D*). On the other hand, the transport of riboflavin by hRFT1 and hRFT3 was independent of extracellular pH, whereas that by hRFT2 was sensitive (Fig. 6). These results suggested that the transport mechanism of hRFT2 differs from those of hRFT1 and hRFT3. Moreover, hRFT2 has 42.9 and 44.1% identity with hRFT1 and hRFT3, respectively, although hRFT1 and hRFT3 exhibit 86.7% identity (Supplemental Fig. 1). From the functional characterizations and sequence analyses, hRFT1 and hRFT3, but not hRFT2, have similar characteristics.

hRFT1 and hRFT2 were strongly expressed in the small intestine (Fig. 2). The characteristics of hRFT2 are similar to the carrier-mediated riboflavin uptake from the apical side of the Caco-2 human intestinal epithelial cells in terms of the affinity for riboflavin, Na^+-dependency, pH-dependency, and substrate specificity (Figs. 5*C*, 6, 7*C*; Supplemental Fig. 2*A*) (20). These data, however, contradict previous reports using small intestinal tissue specimens and brush border membrane vesicles from the perspective of Na^+-dependency (21–26). On the other hand, the uptake of riboflavin by the basolateral membrane vesicles isolated from the small intestine was independent of Na^+ and pH (27); therefore, the features of hRFT1 resemble those of the basolateral membrane (Fig. 6; Supplemental Fig. 2*A*). Although further studies about the membrane localization and the driving force of hRFT1 and hRFT2 are needed, the present findings suggest that 2 different types riboflavin transporters, hRFT1 and hRFT2, play cooperative roles in riboflavin transport in the small intestine.

Riboflavin consists of an isoalloxazine ring and ribose side chain and is converted to 2 coenzyme forms, FMN and FAD, in the cell. FMN has a phosphate group attached to the α carbon of the ribityl side chain, and FAD has ADP attached at the ribose moiety. Its photolytic degradation product, lumiflavine, has a methyl group substituting for the ribose side chain. The chemical structures of these analogs are shown in Figure 7*A*. The transport activity of hRFT was completely inhibited by lumiflavine, but not D-ribose (Fig. 7*B*–*D*), suggesting that the isoalloxazine ring of riboflavin, but not the ribose side chain, is necessary for recognition of all hRFT. In addition, the inhibitory effect of FMN on riboflavin transport was stronger than that of FAD, but weaker than that of unlabeled riboflavin. Therefore, the addition of phosphate and ADP to riboflavin could disturb its binding to all hRFT. The substrate specificities of hRFT were similar and relatively specific for riboflavin, as shown in this study and previously reported (Fig. 7) (3,8). hRFT might specifically recognize the isoalloxazine ring of riboflavin as the substrate.

In conclusion, we isolated a new human riboflavin transporter, hRFT3, which could play an important role in riboflavin homeostasis of the brain. hRFT3 is similar to hRFT1, but not to hRFT2, in amino acid sequence homology and functional characteristics. The present study provides important information about the involvement of hRFT in the homeostasis of riboflavin.

Acknowledgments

A.Y., S.M., and T.K. designed the research; Y.Y., A.Y., and H.Y. conducted the research and analyzed the data; Y.Y., A.Y., and H.Y. wrote the paper; S.M., T.K., and K.I. provided critical review of the paper; and K.I. had primary responsibility for final content. All authors read and approved the final manuscript.

Literature Cited

1. Powers HJ. Riboflavin (vitamin B-2) and health. Am J Clin Nutr. 2003;77:1352–60.
2. Foraker AB, Khantwal CM, Swaan PW. Current perspectives on the cellular uptake and trafficking of riboflavin. Adv Drug Deliv Rev. 2003;55:1467–83.
3. Yonezawa A, Masuda S, Katsura T, Inui K. Identification and functional characterization of a novel human and rat riboflavin transporter, RFT1. Am J Physiol Cell Physiol. 2008;295:C632–41.
4. Hirokawa T, Boon-Chieng S, Mitaku S. SOSUI: classification and secondary structure prediction system for membrane proteins. Bioinformatics. 1998;14:378–9.
5. Burgess CM, Slotboom DJ, Geertsma ER, Duurkens RH, Poolman B, van Sinderen D. The riboflavin transporter RibU in Lactococcus lactis: molecular characterization of gene expression and the transport mechanism. J Bacteriol. 2006;188:2752–60.
6. Vitreschak AG, Rodionov DA, Mironov AA, Gelfand MS. Regulation of riboflavin biosynthesis and transport genes in bacteria by transcriptional and translational attenuation. Nucleic Acids Res. 2002;30:3141–51.
7. Reihl P, Stolz J. The monocarboxylate transporter homolog Mch5p catalyzes riboflavin (vitamin B2) uptake in Saccharomyces cerevisiae. J Biol Chem. 2005;280:39809–17.
8. Yamamoto S, Inoue K, Ohta K, Fukatsu R, Maeda J, Yoshida Y, Yuasa H. Identification and functional characterization of rat riboflavin transporter 2. J Biochem. 2009;145:437–43.
9. Motohashi H, Sakurai Y, Saito H, Masuda S, Urakami Y, Goto M, Fukatsu A, Ogawa O, Inui K. Gene expression levels and immunolocalization of organic ion transporters in the human kidney. J Am Soc Nephrol. 2002;13:866–74.
10. Urakami Y, Akazawa M, Saito H, Okuda M, Inui K. cDNA cloning, functional characterization, and tissue distribution of an alternatively spliced variant of organic cation transporter hOCT2 predominantly expressed in the human kidney. J Am Soc Nephrol. 2002;13:1703–10.
11. Farrell CL, Pardridge WM. Blood-brain barrier glucose transporter is asymmetrically distributed on brain capillary endothelial lumenal and ablumenal membranes: an electron microscopic immunogold study. Proc Natl Acad Sci USA. 1991;88:5779–83.
12. Thorens B, Sarkar HK, Kaback HR, Lodish HF. Cloning and functional expression in bacteria of a novel glucose transporter present in liver, intestine, kidney, and beta-pancreatic islet cells. Cell. 1988;55:281–90.
13. Fukumoto H, Seino S, Imura H, Seino Y, Eddy RL, Fukushima Y, Byers MG, Shows TB, Bell GI. Sequence, tissue distribution, and chromosomal localization of mRNA encoding a human glucose transporter-like protein. Proc Natl Acad Sci USA. 1988;85:5434–8.
14. Sotiriou S, Gispert S, Cheng J, Wang Y, Chen A, Hoogstraten-Miller S, Miller GF, Kwon O, Levine M, et al. Ascorbic-acid transporter Slc23a1 is essential for vitamin C transport into the brain and for perinatal survival. Nat Med. 2002;8:514–7.
15. Tsukaguchi H, Tokui T, Mackenzie B, Berger UV, Chen XZ, Wang Y, Brubaker RF, Hediger MA. A family of mammalian Na^+-dependent L-ascorbic acid transporters. Nature. 1999;399:70–5.
16. Nagatsu T, Nagatsu-Ishibashi I, Okuda J, Yagi K. Incorporation of peripherally administered riboflavine into flavine nucleotides in the brain. J Neurochem. 1967;14:207–10.
17. Spector R, Boose B. Active transport of riboflavin by the isolated choroid plexus in vitro. J Biol Chem. 1979;254:10286–9.
18. Burch HB, Combs AM, Lowry OH, Padilla AM. Effects of riboflavin deficiency and realimentation on flavin enzymes of tissues. J Biol Chem. 1956;223:29–45.
19. Spector R. Riboflavin accumulation by rabbit brain slices in vitro. J Neurochem. 1980;34:1768–71.

20. Said HM, Ma TY. Mechanism of riboflavine uptake by Caco-2 human intestinal epithelial cells. Am J Physiol Gastrointest Liver Physiol. 1994;266:G15–21.
21. Hegazy E, Schwenk M. Riboflavin uptake by isolated enterocytes of guinea pigs. J Nutr. 1983;113:1702–7.
22. Said HM, Arianas P. Transport of riboflavin in human intestinal brush border membrane vesicles. Gastroenterology. 1991;100:82–8.
23. Daniel H, Rehner GL. Sodium-dependent transport of riboflavin in brush border membrane vesicles of rat small intestine is an electrogenic process. J Nutr. 1992;122:1454–61.
24. Tomei S, Yuasa H, Inoue K, Watanabe J. Transport functions of riboflavin carriers in the rat small intestine and colon: site difference and effects of tricyclic-type drugs. Drug Deliv. 2001;8:119–24.
25. Middleton HM. Uptake of riboflavin by rat intestinal mucosa in vitro. J Nutr. 1990;120:588–93.
26. Daniel H, Wille U, Rehner G. In vitro kinetics of the intestinal transport of riboflavin in rats. J Nutr. 1983;113:636–43.
27. Said HM, Hollander D, Mohammadkhani R. Uptake of riboflavin by intestinal basolateral membrane vesicles: a specialized carrier-mediated process. Biochim Biophys Acta. 1993;1148:263–8.

Journal of Gastroenterology and Hepatology

JGHF

doi:10.1111/j.1440-1746.2009.06206.x

GASTROENTEROLOGY

Efficacy and safety of infliximab as rescue therapy for ulcerative colitis refractory to tacrolimus

Shuji Yamamoto,*,† Hiroshi Nakase,* Minoru Matsuura,* Yusuke Honzawa,* Satohiro Masuda,‡ Ken-ichi Inui‡ and Tsutomu Chiba*

*Department of Gastroenterology and Hepatology, Graduate School of Medicine, Kyoto University, Kyoto, †Research Fellow of the Japan Society for the Promotion of Science, Tokyo, and ‡Department of Pharmacy, Kyoto University Hospital, Kyoto, Japan

Key words
infliximab, tacrolimus, ulcerative colitis.

Accepted for publication 16 November 2009.

Correspondence
Dr Hiroshi Nakase, Department of Gastroenterology and Hepatology, Graduate School of Medicine, Kyoto University, 54 Shogoin Kawahara-cho, Sakyo-ku, Kyoto 606-8507, Japan. Email: hiropy_n@kuhp.kyoto-u.ac.jp

Abstract

Background and Aim: Little is known about the efficacy and safety of infliximab for ulcerative colitis refractory to tacrolimus. The aim of this study was to evaluate the efficacy and safety of infliximab in the induction of remission in ulcerative colitis patients with persistent symptoms despite tacrolimus therapy.

Methods: We report a retrospective, observational, single-center case series of 12 consecutively enrolled patients with ulcerative colitis refractory to tacrolimus that received infliximab therapy for the induction of remission. Eight patients received a single infusion of infliximab, and four received two or more infusions. Median follow-up duration was 16.0 months (range, 1.6–41.4 months). The clinical response was evaluated based on a modified Truelove-Witts severity index.

Results: Six patients (50.0%) achieved clinical remission within 30 days. Overall cumulative colectomy-free survival was estimated to be 58.3% at 41.4 months. Adverse events included an elevation of liver enzymes (1/12; 8.3%) and a mild infusion reaction (1/12; 8.3%). No mortality occurred.

Conclusions: Infliximab can induce remission in patients with ulcerative colitis who do not tolerate or respond to tacrolimus therapy.

Introduction

Ulcerative colitis (UC) is an idiopathic, chronic, and inflammatory disorder characterized by diarrhea, rectal bleeding, abdominal pain, fever, anemia, and body weight loss.[1] Corticosteroid therapy is used for patients with UC who do not respond to aminosalicylates or those with a severe attack of UC.[1–3] Although most patients with UC initially respond to corticosteroids, approximately 20% of patients with UC become steroid-dependent and 30% of those require surgery within 1 year after initiating corticosteroid therapy.[4]

Tacrolimus is reported to be effective for patients with ulcerative colitis (UC) refractory to steroids. One placebo-controlled study[1] and several uncontrolled studies[6–10] demonstrated the short-term efficacy of tacrolimus treatment in patients with UC, and there are several reports on the long-term effects.[6–8] Recently, we demonstrated both the short- and long-term efficacy of tacrolimus for refractory UC.[11] In that study, 21 of 27 (77.8%) patients had a clinical response and overall cumulative colectomy-free survival was 62.3% at 65 months.[11] Some patients with refractory UC, however, do not have a clinical response to tacrolimus or relapse even after clinical remission with tacrolimus therapy is achieved.

Infliximab (IFX) is a chimeric IgG1 monoclonal antibody to tumor necrosis factor-alpha (TNFα) that binds with high affinity to TNFα, neutralizing its biologic activity.[12] The Active Ulcerative Colitis Trials (ACT) 1 and 2 proved the efficacy of IFX in inducing and maintaining a clinical response and remission in patients with moderate or severe UC.[13] In patients who received IFX, 61% to 69% had a clinical response at week 8, while 29% to 37% of those who received placebo had a clinical response in these studies. In ACT 1, a clinical response was achieved at week 54 in significantly more patients who received IFX than those who received placebo.

Patients with steroid-refractory UC who failed second-line therapies with cyclosporine, tacrolimus, or IFX have limited medical options to achieve remission and avoid colectomy. Recently, the effect of IFX as rescue therapy on patients with steroid-refractory UC who did not respond to cyclosporine was reported by two groups. Maser *et al.*[14] demonstrated that four (40%) of 10 patients achieved remission, two (20%) responded to IFX therapy, and six (60%) avoided colectomy or death during an average follow-up period of 7.8 months. Mañosa *et al.*[15] reported that 10 (62.5%) of 16 patients avoided colectomy during median follow-up from the first IFX infusion of 195 days.